Urban Climate 65 (2026) 102836

Contents lists available at ScienceDirect

Urban Climate

journal homepage: www.elsevier.com/locate/uclim

Parametric optimization of urban residential morphology for outdoor thermal comfort with integrated code regulatory and site development requirement☆

Pengyuan Shen [a,*], Xiaoni Gao [a], Yuting Liu [b], Yi Zhang [a], Xing Zheng [c]

[a] *Institute of Future Human Habitats, Shenzhen International Graduate School, Tsinghua University, Shenzhen, Guandong Province, China*
[b] *School of Architecture, Harbin Institute of Technology, Shenzhen, Guandong Province, China*
[c] *Department of Architecture and Civil Engineering, City University of Hong Kong, Hong Kong, SAR, China*

ARTICLE INFO

Keywords:
Urban morphology
Parametric optimization
Residential neighborhood
Outdoor thermal comfort
UTCI
Hot-humid climate

ABSTRACT

Urban heat island phenomena pose threats to outdoor thermal comfort in high-density residential areas in hot-humid climatic cities. This study presented an integrated parametric optimization framework that combined empirical data collection, environmental simulation and multi-objective genetic algorithms in order to improve the thermal comfort in residential neighborhoods. Based on the morphological structure of 972 residential areas located in Shenzhen's four central districts, morphological parameter ranges were defined for three basic layouts: row style, cluster style, and courtyard style. Using Rhino+Grasshopper platform, parametric models were created and optimized using coupled thermal comfort (UTCI), wind environment, and daylighting performance simulations. AIJ case and field validation was performed to ensure model accuracy. Multi-objective optimization demonstrated that thermal comfort can be improved by 0.2–0.6 °C UTCI with daylighting compliance imposed. The best values of mean UTCI for normal conditions in a summer week were found to be 31.66–33.05 °C for all configurations in comparison with 32.19–33.53 °C for worst-case scenarios. Regression analysis showed that the parameter sensitivities were layout dependent with cluster-style configurations showing strongest correlation (R^2 = 0.398–0.625) between morphological variables and thermal performance. The application of the Bao'an district case study in Shenzhen also confirmed practical applicability in good integration with local regulatory limitations.

1. Introduction

Urban heat island (UHI) effects have emerged as a critical environmental challenge in high-density cities worldwide, with outdoor thermal comfort deterioration becoming increasingly pronounced in hot-humid climate regions (Shi and Zhang, 2022). Rapid urbanization processes, characterized by extensive building construction and reduced green spaces, have significantly intensified local heat accumulation and compromised natural ventilation patterns, particularly affecting residential neighborhoods where citizens spend substantial portions of their daily lives (Morris et al., 2017; Yuan et al., 2022). Concurrent with urbanization, climate change projections indicate continued warming trends in subtropical regions, with mean temperatures expected to rise, further exacerbating

☆ This article is part of a Special issue entitled: 'Local climate and energy in the built environment' published in Urban Climate.

* Corresponding author.
E-mail address: pengyuan_pub@163.com (P. Shen).

https://doi.org/10.1016/j.uclim.2026.102836
Received 8 October 2025; Received in revised form 7 January 2026; Accepted 12 February 2026
Available online 17 February 2026

Nomenclature

Symbol

UHI	Urban Heat Island (—)
UTCI	Universal Thermal Climate Index (°C)
PET	Physiological Equivalent Temperature (°C)
PMV	Predicted Mean Vote (—)
MRT	Mean Radiant Temperature (°C)
CFD	Computational Fluid Dynamics (—)
RANS	Reynolds-Averaged Navier-Stokes (—)
LES	Large Eddy Simulation (—)
GA	Genetic Algorithm (—)
NSGA-II	Non-dominated Sorting Genetic Algorithm II (—)
PSO	Particle Swarm Optimization (—)
FAR	Floor Area Ratio (—)
AIJ	Architectural Institute of Japan (—)
TMY	Typical Meteorological Year (—)
GIS	Geographic Information System (—)
IoA	Index of Agreement (—)
RMSE	Root Mean Square Error (—)
HR-I	High-rise Type I (19–33 floors) (—)
HR-II	High-rise Type II (10–18 floors) (—)
Multi	Multi-story (4–9 floors) (—)

Parameters

T_{air}	Air temperature (°C)
T_{surf}	Surface temperature (°C)
T_{mrt}	Mean radiant temperature (K)
ΔT_{UTCI}	UTCI offset from air temperature (°C)
I_{solar}	Total solar irradiance on surface (W/m$^{2)}$
α	Solar absorptance (—)
h_c	Convective heat transfer coefficient (W/(m^2·K))
h_r	Radiative heat transfer coefficient (W/(m^2·K))
$F_{i\text{-}j}$	View factor between surfaces i and j (—)
U(z)	Wind velocity at height z (m/s)
u^*	Friction velocity (m/s)
κ	von Kármán constant (0.41) (—)
z	Height above ground (m)
z_0	Surface roughness length (m)
H	Building height (m)
S_i	Simulated value (—)
M_i	Measured value (—)
d	Consistency index (—)
R^2	Coefficient of determination (—)
η	Distribution index for genetic operators (—)
n	Number of design variables (—)

outdoor thermal stress in already heat-vulnerable urban environments (Shen et al., 2025a). The compounding effects of climate change and urban densification have created thermal environments that frequently exceed human comfort thresholds, leading to reduced outdoor activity levels, increased energy consumption for cooling, and adverse public health impacts (Shen et al., 2025a; Chen and Ng, 2012; Shen et al., 2025b).

Traditional residential neighborhood design approaches predominantly rely on empirical knowledge and regulatory compliance, often failing to adequately address the complex interactions between building morphology and microclimate performance (Kamal et al., 2021). Conventional planning methods typically prioritize land use efficiency and functional organization while treating thermal comfort as a secondary consideration, resulting in suboptimal environmental outcomes that become evident only after construction completion(Givoni, 1998). This reactive approach limits opportunities for climate-responsive design interventions and perpetuates the development of thermally uncomfortable urban environments, particularly in regions where cooling demands are substantial and persistent throughout extended summer periods under ongoing climate change (Giannakopoulos et al., 2005).

The integration of computational design tools and performance-based optimization methods presents unprecedented opportunities to revolutionize residential neighborhood planning through evidence-based decision-making processes (Cui et al., 2025; Li et al., 2024). Parametric modeling platforms, coupled with environmental simulation capabilities and multi-objective optimization algorithms, enable designers to systematically explore vast design solution spaces while simultaneously evaluating multiple performance criteria (Roudsari et al., 2013; Yi and Malkawi, 2009). This computational paradigm shift facilitates the development of climate-adaptive urban forms that can effectively balance thermal comfort requirements with other essential planning objectives, including daylighting quality, natural ventilation, and regulatory compliance (Pan and Du, 2022; Yuan and Ng, 2012).

This research develops a comprehensive parametric optimization framework for residential neighborhood morphology in hot-humid climates, using Shenzhen as a representative case study. The methodology integrates three-dimensional parametric modeling, coupled environmental simulations encompassing thermal comfort (UTCI), wind environment, and daylighting performance, with genetic algorithm-based multi-objective optimization. Research objectives include establishing quantitative relationships between morphological parameters and outdoor thermal comfort, developing automated design optimization workflows incorporating regulatory constraints, and deriving evidence-based design strategies for row-style, cluster-style, and courtyard-style residential layouts. This study provides urban planners and architects with scientific tools for creating comfortable, energy-efficient residential environments while demonstrating practical feasibility of integrating advanced computational methods into conventional planning workflows.

2. Literature review

Outdoor thermal comfort research has evolved significantly over the past decades, transitioning from simple temperature-based assessments to comprehensive multi-parameter evaluations that consider human physiological and psychological responses to environmental conditions. The Universal Thermal Climate Index (UTCI) has emerged as the most widely adopted metric for outdoor thermal comfort assessment (Ji et al., 2022), integrating air temperature, relative humidity, wind speed, and mean radiant temperature with human thermal physiology models (Fiala et al., 2012). UTCI's superiority over traditional indices such as Physiological Equivalent Temperature (PET) (Hoppe, 1999) and Predicted Mean Vote (PMV) (Ku et al., 2015) lies in its universal applicability across diverse climatic conditions and its ability to account for clothing insulation and metabolic rate variations (Błażejczyk et al., 2013). Recent studies have validated UTCI's effectiveness in hot-humid climates, demonstrating strong correlations between calculated values and subjective thermal sensation votes in tropical urban environments (Deng et al., 2022; Zhen et al., 2022). Field studies in Southeast Asian cities have confirmed that UTCI provides more accurate predictions of thermal sensation compared to simplified heat indices, particularly during extreme weather conditions when multiple environmental factors interact to influence human thermal perception (Lai et al., 2014).

The relationship between urban morphology and microclimate has been extensively investigated, revealing complex interactions between building configurations and thermal environment characteristics. Building density and layout patterns significantly influence air temperature, wind patterns, and solar radiation distribution within urban spaces (Oke et al., 2017). High-density developments often create canyon effects that trap heat and reduce wind speeds, while strategic building arrangements can enhance natural ventilation and provide beneficial shading (Ali-Toudert and Mayer, 2006). Research in hot climates has demonstrated that building height-to-width ratios, street orientations, and courtyard configurations critically affect outdoor thermal comfort, with optimal configurations varying according to local climate characteristics (Kedissa et al., 2016; Yang et al., 2022). The orientation of building facades relative to prevailing winds and solar paths plays a crucial role in determining outdoor thermal conditions, with north-south oriented streets generally providing better thermal comfort in tropical regions (Akpan, 2023). Studies of traditional courtyard housing in hot climates have revealed that enclosed spaces can effectively moderate extreme temperatures through strategic shading and wind channeling effects, though optimal courtyard proportions differ significantly between dry and humid climates (Soflaei et al., 2017). The concept of urban porosity, defined as the ratio of void spaces to total urban volume, has gained attention as a critical parameter for enhancing natural ventilation and reducing heat accumulation in dense urban environments (Yuan and Ng, 2012; Ng et al., 2011).

Parametric design methodologies have revolutionized architectural and urban planning practices by enabling systematic exploration of design alternatives through computational algorithms (Çalışkan, 2017). Grasshopper and similar visual programming platforms have become standard tools for generating complex geometries while maintaining parametric relationships between design variables (Davidson, 2013; Khan, 2024). These tools facilitate rapid iteration and evaluation of multiple design scenarios, allowing designers to investigate performance implications of morphological variations (Yi and Malkawi, 2009; Taleb and Musleh, 2015). The integration of parametric modeling with environmental simulation tools has created powerful workflows for performance-driven design, enabling real-time feedback on thermal, lighting, and energy performance (Evins, 2013; Nguyen et al., 2014). Recent developments in cloud-based computation have further enhanced the accessibility and processing power available for complex urban-scale parametric studies (Bre and Gimenez, 2022). Advanced parametric design methods now incorporate machine learning algorithms that can identify optimal design patterns from large datasets, reducing computational time while maintaining solution quality (Feng et al., 2019). The emergence of generative design approaches, which combine parametric modeling with artificial intelligence, has opened new possibilities for discovering innovative urban forms that respond to multiple environmental constraints simultaneously (Zheng and Yuan, 2021).

Multi-objective optimization techniques have gained prominence in architectural applications due to their ability to simultaneously address conflicting design objectives such as thermal comfort, energy efficiency, and spatial functionality (Du et al., 2020; Shen, 2024). Genetic algorithms (GA) have proven particularly effective for architectural optimization problems due to their ability to handle non-linear relationships and discontinuous design spaces (Asadi et al., 2014; Caldas and Norford, 2002). The Non-dominated Sorting Genetic Algorithm II (NSGA-II) has become a standard approach for multi-objective optimization in building design, providing well-distributed Pareto frontiers that represent optimal trade-offs between competing objectives (Carlucci et al., 2015). Particle swarm optimization (PSO) and differential evolution algorithms have also shown promise in urban planning applications, offering alternative approaches to complex optimization problems (Masoomi et al., 2013). The Non-dominated Sorting Differential Evolution algorithm (NSDE) has been used to optimize lifecycle solutions for building retrofit problems considering climate change impacts (Shen, 2024). The integration of machine learning techniques with evolutionary algorithms has opened new possibilities for accelerating optimization processes and improving solution quality (Cui et al., 2025). Recent advances include hybrid optimization approaches that combine global search algorithms with local refinement methods, achieving superior performance in complex urban design problems (Li et al., 2022a). Multi-criteria decision-making frameworks integrated with machine learning methods have been developed to assist designers in selecting optimal solutions from Pareto sets, incorporating stakeholder preferences and regulatory constraints into the decision process (Shen, 2024; Machairas et al., 2014).

Climate-responsive design principles emphasize the adaptation of building forms and urban layouts to local climatic conditions, drawing inspiration from vernacular architecture and bioclimatic design traditions (Shen et al., 2025a; Givoni, 1998; Olgyay, 2016) (Moazami et al., 2019). Moreover, the concept of adaptive thermal comfort recognizes that occupants in naturally ventilated environments can tolerate wider temperature ranges through behavioral and physiological adaptations, influencing acceptable thermal comfort ranges in indoor spaces (de Dear and Brager, 2002). Traditional passive cooling strategies from vernacular buildings, such as raised floors, deep overhangs, and cross-ventilation, have been reinterpreted through contemporary computational design methods to create climate-responsive urban forms (Li et al., 2022b; Zhai and Previtali, 2010). Recent investigations have further advanced the understanding of climate-responsive design through diverse methodological approaches. Alinasab et al.'s study integrated machine learning with morphological dynamics and demonstrated enhanced prediction capabilities for outdoor thermal regulation in complex urban environments based on field measurement in 173 urban canyons (Alinasab et al., 2025). Research examining green space structure impacts on physiological equivalent temperature (PET) has quantified vegetation contributions to thermal comfort in open spaces (Davtalab et al., 2020), while parametric simulation studies have evaluated the effects of design parameter including building height, orientation and urban geometry, on urban overheating and outdoor thermal conditions (Wai et al., 2024). Combined thermal comfort prediction models based on UTCI, PET and SET models, which incorporates multiple environmental variables, have improved assessment accuracy in Rome (Pompei et al., 2024). A systematic reviews of outdoor thermal comfort research have synthesized design principles for urban square redevelopment, which pointed out that there is no establishment of dedicated local models for thermal comfort analysis and improvement for city squares (Mandić et al., 2024). Furthermore, studies of vernacular architecture in hot arid regions, particularly examining traditional elements such as Kharkhona in Sistan housing, have demonstrated effective passive strategies for humidity regulation, wind speed modification, and temperature adjustment that inform contemporary sustainable design approaches (Kiani et al., 2025; Heydari and Davtalab, 2020). Climate-responsive design frameworks developed for hot arid urban open spaces can provide complementary insights applicable to hot-humid contexts through adaptation of shading and ventilation strategies (Alharthi et al., 2025).

The integration of vegetation and water features in urban design has been quantified through microclimatic studies, demonstrating significant cooling effects that can reduce ambient temperatures in tropical environments (Broadbent et al., 2018; Dimoudi and Nikolopoulou, 2003). Computational fluid dynamics (CFD) simulation has become an essential tool for predicting wind patterns and thermal conditions in urban environments, providing detailed insights into microclimate variations that influence outdoor thermal comfort (Blocken, 2015). The accuracy of CFD simulations depends critically on boundary condition specifications, turbulence modeling approaches, and grid resolution, with validation against experimental data being essential for reliable predictions (Tominaga et al., 2008). Large Eddy Simulation (LES) has shown superior performance compared to Reynolds-Averaged Navier-Stokes (RANS) models for complex urban flows, though at significantly higher computational costs (Zheng and Yang, 2021; Zheng and Yang, 2022). Recent advances in GPU computing have made high-resolution CFD simulations more accessible for routine design applications, enabling more detailed investigations of urban microclimate (Sauer and Muñoz-Esparza, 2020). Coupled simulation approaches that integrate CFD with building energy models and radiation calculations have emerged as comprehensive tools for evaluating urban environmental performance concerning thermal comfort and air quality (Cui et al., 2026; Wang et al., 2025). The development of reduced-order models and surrogate modeling techniques has addressed computational limitations, enabling real-time optimization workflows suitable for design practice (Ahn et al., 2025; Low et al., 2022).

Despite significant advances in computational tools and optimization methodologies, several research gaps persist in the application of parametric optimization to residential neighborhood design for thermal comfort. Most existing studies focus on simplified geometric configurations or single building performance, with limited investigation of district-scale morphological optimization considering regulatory constraints and practical implementation requirements (Xu et al., 2019). The integration of multiple environmental performance criteria with real-world design constraints remains challenging, particularly in high-density urban contexts where land use efficiency must be balanced against environmental quality (Wang et al., 2024). Furthermore, the transferability of optimization results across different climatic contexts and cultural settings requires further investigation to develop robust design frameworks applicable to diverse urban environments. Limited research has addressed the temporal dynamics of urban microclimates and their implications for year-round thermal comfort optimization, with most studies focusing on peak summer conditions while neglecting shoulder seasons and diurnal variations (Santamouris, 2013).

This research addresses these challenges by developing a comprehensive parametric optimization framework specifically tailored for residential neighborhood morphology in hot-humid climates, using Shenzhen, China, as a representative case study. The methodology integrates three-dimensional parametric modeling, coupled environmental simulations encompassing thermal comfort (UTCI), wind environment, and daylighting performance, with genetic algorithm-based multi-objective optimization to generate climate-responsive design solutions. The research objectives encompass the establishment of quantitative relationships between morphological parameters and outdoor thermal comfort, the development of an automated design optimization workflow that incorporates regulatory constraints, and the derivation of evidence-based design strategies for three typical residential layout configurations: row-style, cluster-style, and courtyard-style arrangements.

The significance of this research extends beyond methodological contributions to encompass practical applications for sustainable urban development in hot-humid regions globally. By providing quantitative insights into the relationships between residential neighborhood morphology and thermal environment performance, this study offers urban planners and architects scientific tools for creating more comfortable and energy-efficient residential environments. The research contributes to the growing body of knowledge in climate-responsive urban design while demonstrating the practical feasibility of integrating advanced computational methods into conventional planning workflows, ultimately supporting the development of more resilient and sustainable urban communities in an era of increasing climate challenges.

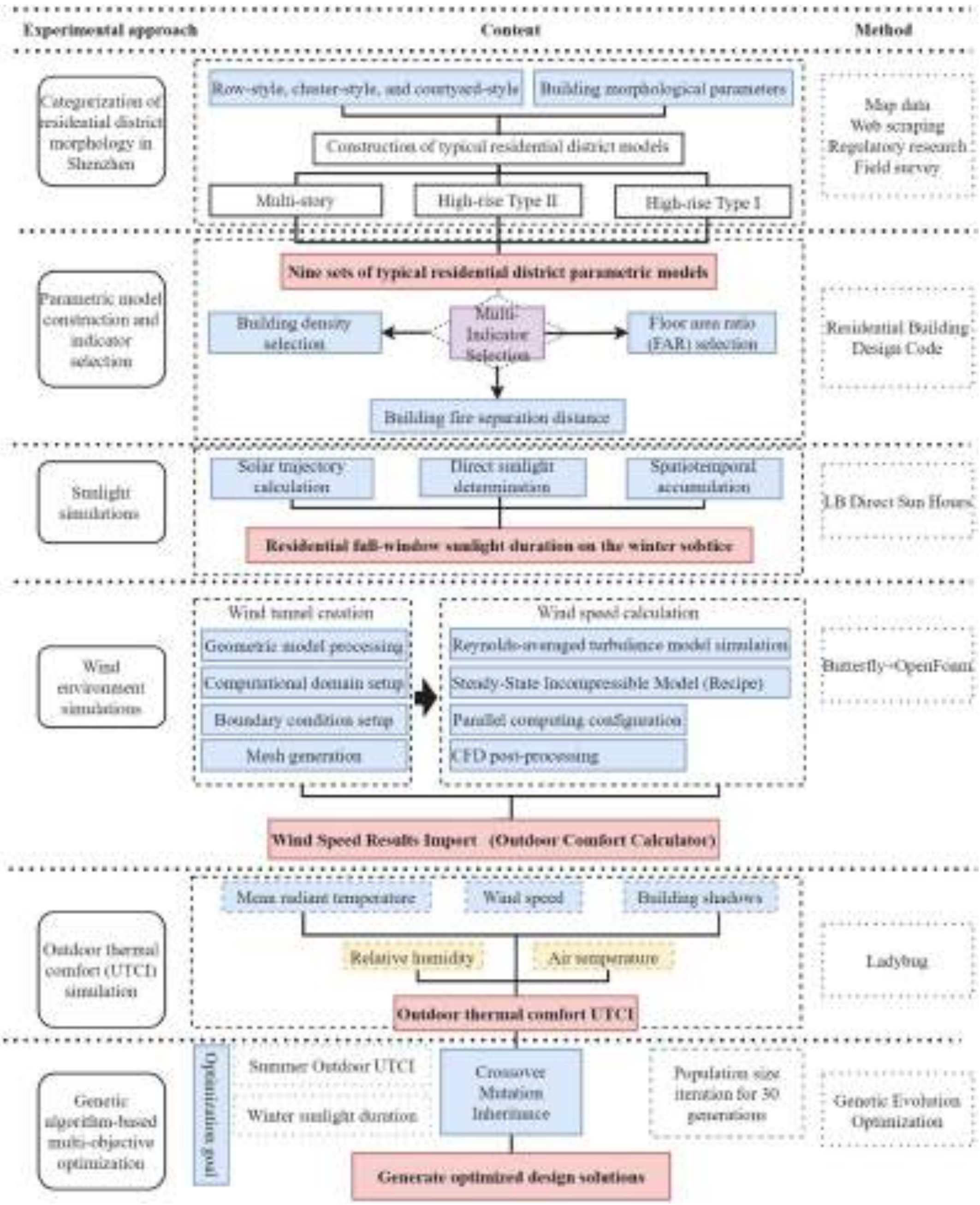

Fig. 1. Research framework of this study.

3. Methodology

3.1. Research framework

This study employs a comprehensive parametric optimization framework that integrates empirical data collection, computational modeling, environmental simulation, and multi-objective optimization to enhance outdoor thermal comfort in residential neighborhoods. The methodology follows a five-stage workflow: (1) field survey and database construction based on Shenzhen's existing residential neighborhoods; (2) parametric model development using Rhino+Grasshopper platform; (3) numerical model validation following international standards; (4) coupled environmental performance simulation incorporating thermal comfort, wind environment, and daylighting analysis; and (5) genetic algorithm-based multi-objective optimization targeting UTCI improvement and regulatory compliance. This integrated approach ensures that optimization results are grounded in real-world constraints while maintaining computational efficiency and practical applicability. The framework bridges the gap between theoretical optimization and practical implementation by incorporating building codes, site constraints, and climate-specific requirements into the computational workflow, enabling the generation of feasible design solutions that can be directly applied to urban planning practice. Fig. 1 shows the research framework of this work.

3.2. Case study area and data collection

The research focuses on Shenzhen, a representative hot-humid climate city in southern China, characterized by high urban density and significant thermal comfort challenges. A comprehensive survey was conducted across four central districts (Futian, Luohu, Nanshan, and Bao'an), covering 972 residential neighborhoods to establish a robust empirical foundation for parametric modeling. The survey procedure is illustrated in Fig. 2. The data collection employed multiple methodologies including web scraping techniques for initial screening, satellite imagery analysis for morphological characterization, and field measurements for validation purposes.

The classification system was established based on China's Building Design Fire Code (GB 50016–2014), categorizing residential developments into three primary types: multi-story (4–9 floors, height ≤ 27 m), high-rise Type II (10–18 floors, 27 m ≤ height ≤ 54 m), and high-rise Type I (19–33 floors, 54 m ≤ height ≤ 100 m). This classification differs from conventional planning standards by emphasizing fire safety requirements, which better reflects actual construction practices in high-density urban environments. Table 1 presents the statistical distribution of building density and floor area ratio (FAR) across different building types, revealing distinct patterns that inform subsequent parametric modeling constraints.

From the initial dataset, 164 representative residential neighborhoods were selected for detailed morphological analysis, encompassing 2031 individual buildings. The selection criteria included: (1) minimum six buildings per district to ensure statistical significance; (2) clear plot boundaries for accurate geometric analysis; (3) construction completion after 2000 to reflect contemporary planning practices; and (4) representative distribution across the three layout typologies. Three dominant layout patterns emerged from the analysis: row-style (29% of samples), cluster-style (38% of samples), and courtyard-style (23% of samples), with mixed layouts comprising the remainder. Table 2 shows samples of specific neighborhoods with different layouts.

Morphological parameters were extracted through GIS analysis and field verification, establishing ranges for key design variables including building width (25–65 m), depth (10-36 m), orientation (−45° to +50° from south), and inter-building spacing. Our database is also incorporated with climate data from Shenzhen Weather Station, providing hourly meteorological records for typical summer weeks and winter solstice conditions essential for subsequent thermal comfort and daylighting simulations.

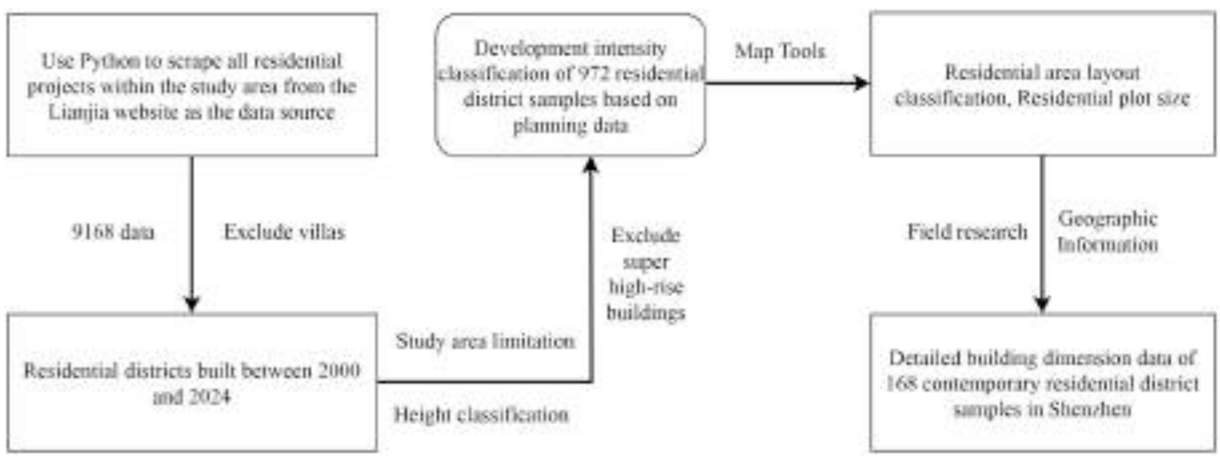

Fig. 2. Residential neighborhood data collection.

Table 1
Building classification standards for residential neighborhoods.

Classification	Floor Range	Floor Area Ratio	Maximum Building Density (%)
Multi-story	4–9	1.0–2.5	35
High-rise Type II	10–18	1.5–4.0	30
High-rise Type I	19–33	2.5–6.0	25

Table 2
Samples of specific neighborhoods with different layouts.

Name	Feature Description	Actual residential neighborhood cases in Shenzhen			
Row-style	Row-style arrangements featuring parallel building alignments			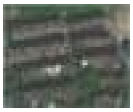	
		Oulu Jingdian Community	Newport Garden	Yuezhong Community	Guangchang North Street Community
			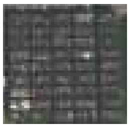	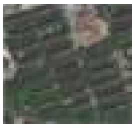	
		Qianhai Era	Minle Garden	Sihai Zhendi	Huaqiang Garden
Cluster-style	Cluster-style configurations with point buildings distributed across regular grids	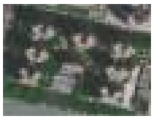		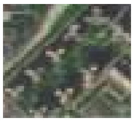	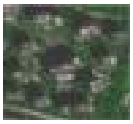
		Peninsula City-State	Mangrove Oasis	Mountainside Garden	Fifteen Peaks Garden
					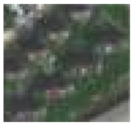
		Jinshan Prefecture	British Garden	Haina Mansion	Nanshan Construction Village
Courtyard-style	Courtyard-style layouts creating enclosed or semi-enclosed spaces				
		Portofino Pure Waterfront	Xinghai Famous City	Dingtai Fenghua	Langqin Island Garden
			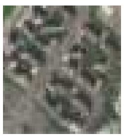		
		Yongcui Mansion	Qianhaiwan Gardens	Guanhaitai Garden	Langlu Home

3.3. Numerical model validation

3.3.1. AIJ standard case validation

Model validation was conducted following the Architectural Institute of Japan (AIJ) guidelines for CFD simulation in urban environments, ensuring computational accuracy and reliability for subsequent optimization studies (Tominaga et al., 2008). The AIJ validation protocol employs standardized test cases with known experimental results, providing benchmark scenarios for assessing CFD model performance under controlled conditions.

The validation process utilized AIJ's wind tunnel experimental data (Case C) for simple building arrays, representing fundamental urban flow patterns relevant to residential neighborhood analysis. Computational domain specifications followed AIJ recommendations: upstream distance of 5H (where H represents building height), downstream distance of 15H, lateral boundaries at 5H, and top boundary at 6H to minimize boundary effects on flow development as shown in Fig. 3.

Mesh independence studies were conducted using three grid resolutions - coarse, medium, and fine grid (all in hexahedral mesh), to establish optimal computational efficiency while maintaining solution accuracy. The k-ε turbulence model was selected based on AIJ recommendations for urban flow simulations, with enhanced wall treatment near building surfaces. Boundary conditions specified logarithmic wind profiles at the inlet, zero-gradient conditions at the outlet, and no-slip conditions on building and ground surfaces. Validation results demonstrated progressive improvement in accuracy with mesh refinement, which will be analyzed and discussed later.

3.3.2. In-situ field measurement and validation

Additional validation was performed using field measurements from the Bao'an district study site to confirm model reliability under actual urban conditions. Two micro-environmental monitoring stations were deployed using AG-WZ07 equipment to collect continuous meteorological data during typical summer conditions in July 2025. Table 3 shows the detailed information on the equipment being used for onsite monitoring.

Monitoring Station 1 was positioned near Baosheng Hospital within a green corridor, representing a semi-open urban environment with moderate building density. Station 2 was located in the central pedestrian area of Anle Garden residential complex, characterized by higher building density and more enclosed spatial conditions, which is shown in Fig. 4 (a). Both stations recorded wind speed, temperature, and humidity data at 1.5 m height to correspond with pedestrian-level conditions used in thermal comfort calculations.

Validation metrics include:

$$RMSE = \sqrt{\frac{1}{n}\sum_{i=1}^{n}(S_i - M_i)^2} \tag{1}$$

$$d = 1 - \frac{\sum_{i=1}^{n}(S_i - M_i)^2}{\sum_{i=1}^{n}(|S_i - \overline{M}| + |M_i - \overline{M}|)^2} \tag{2}$$

where S_i represents simulated values, M_i represents measured values, and $\overline{M}$ represents the mean of measured values. The consistency index d ranges from 0 to 1, with values above 0.8 indicating excellent agreement.

3.4. Parametric modeling framework

The parametric modeling framework was developed using Rhino3D and Grasshopper platforms, enabling automated generation of residential neighborhood configurations with precise control over morphological parameters. The system integrates geometric modeling, regulatory compliance checking, and performance simulation within a unified computational environment, facilitating rapid exploration of design alternatives while maintaining adherence to building codes and planning regulations.

Three distinct layout typologies were parameterized based on empirical analysis: row-style arrangements featuring parallel building alignments optimized for daylighting and natural ventilation; cluster-style configurations with point buildings distributed across regular grids to maximize spatial openness; and courtyard-style layouts creating enclosed or semi-enclosed spaces that balance privacy with environmental performance. Each typology incorporates specific geometric constraints derived from the morphological database, ensuring that generated configurations reflect realistic design scenarios.

The parametric framework employs hierarchical constraint systems operating at multiple scales. Site-level constraints establish plot

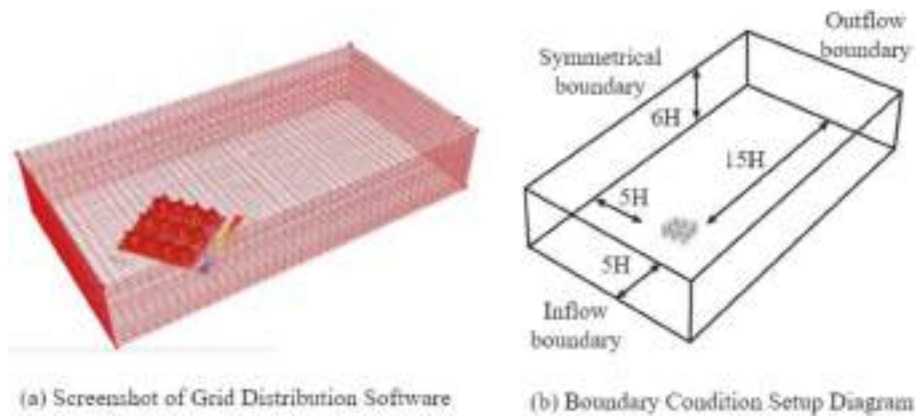

Fig. 3. CFD modeling and validation against AIJ case C.

Table 3
Experimental equipment specifications and parameters.

Equipment Name	Measurement Parameters	Range and Accuracy
Micro Environmental Air Quality Online Monitoring System Model: AG-WZ07	Outdoor Air Temperature (requires radiation shield)	−20–80 °C, ±0.3 °C
	Outdoor Air Humidity (requires radiation shield)	0–100%RH, ±2%RH
	Wind Direction	30–360°, ±2°
	Wind Speed	0–60 m/s, ±0.3 m/s
	Atmospheric Pressure	100 ~ 1200mb, ±0.5 hPa
	Total Solar Radiation	0–2000 W/m^2, ±10 W/m^2
	Diffuse Solar Radiation	20–80 °C, ±0.3°C
	Outdoor Black Globe Temperature (150 mm)	−50 °C ~ +100 °C, ±0.3 °C
	Road, Building, Plaza Surface Temperature	−25–100 °C
	Road, Building, Plaza Heat Transfer Coefficient	>0.02 W/(m·K), ±0.2 °C

Fig. 4. Locations of onsite monitoring station and their surrounding environment.

boundaries, setback requirements (9 m from property lines per Shenzhen regulations), and infrastructure easements. District-level constraints control overall building density, floor area ratios, and open space requirements based on classification standards. Building-level constraints govern individual structure dimensions, orientations, and spacing to ensure fire safety compliance and regulatory conformance. The parametric generation process is illustrated in Fig. 5 and Fig. 6, with design variable ranges summarized in Table 4.

The automated compliance checking system evaluates generated configurations against multiple criteria including minimum building separation distances, fire access requirements, and daylighting standards. Buildings failing to meet winter solstice daylighting requirements (minimum 1 h between 9:00–15:00) are automatically excluded from optimization populations, ensuring that all candidate solutions maintain basic habitability standards. Similarly, configurations exceeding maximum building density or floor area ratio limits are filtered out during the generation process, reducing computational overhead in subsequent optimization stages.

3.5. *Environmental performance simulation*

Environmental performance simulation integrates multiple physical phenomena affecting outdoor thermal comfort, combining thermal analysis, wind environment modeling, and daylighting evaluation within a comprehensive assessment framework. The simulation workflow utilizes specialized software tools optimized for urban-scale environmental analysis, ensuring computational efficiency while maintaining physical accuracy. The complete environmental performance simulation workflow is presented in Fig. 7.

3.5.1. *UTCI calculation*

UTCI calculation employs the Ladybug Tools suite, implementing the complete UTCI computational model including human thermal physiology, clothing insulation, and metabolic rate considerations (Roudsari et al., 2013). Climate data processing utilizes

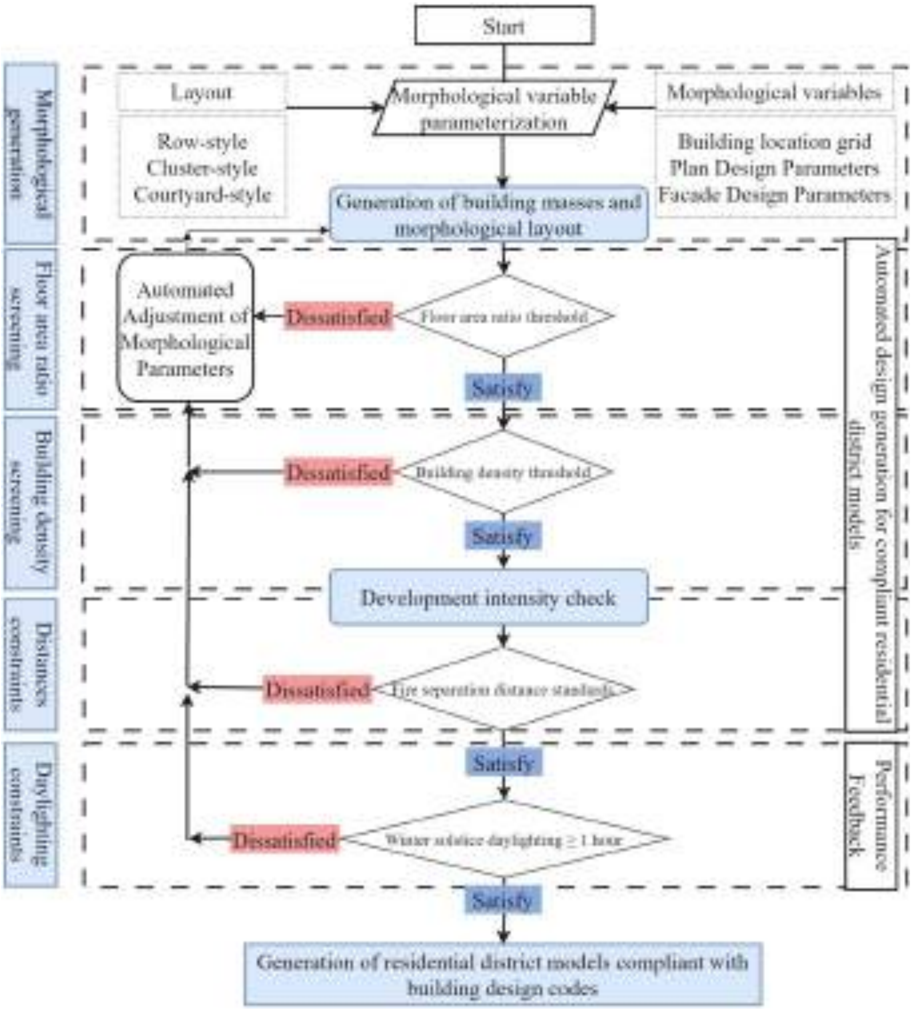

Fig. 5. Generation of residential planning schemes - automatic code compliance verification - parametric performance review system.

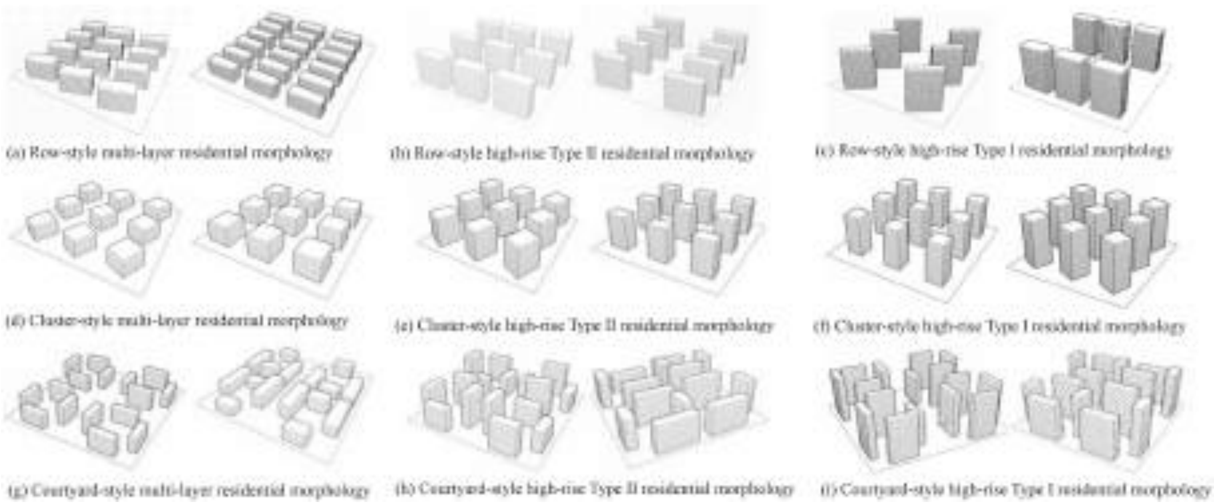

Fig. 6. Parametric generation of neighborhood layout with constraints.

Table 4
Parametric model design variable ranges.

Layout Type	Building Type	Width (m)	Depth (m)	Floors	Rotation (°)	FAR
Row-style	Multi-story	40–60	12–24	4–9	−45 to 50	1.0–2.5
Row-style	High-rise II	40–60	12–24	10–18	−45 to 50	1.5–4.0
Row-style	High-rise I	40–60	12–24	19–33	−45 to 50	2.5–6.0
Cluster-style	Multi-story	25–40	15–36	4–9	−45 to 50	1.0–2.5
Cluster-style	High-rise II	25–40	15–36	10–18	−45 to 50	1.5–4.0
Cluster-style	High-rise I	25–40	15–36	19–33	−45 to 50	2.5–6.0
Courtyard-style	Multi-story	30–60	10–21	4–9	–	1.0–2.5
Courtyard-style	High-rise II	30–60	15–25	10–18	–	1.5–4.0
Courtyard-style	High-rise I	35–65	12–25	19–33	–	2.5–6.0

Shenzhen's TMY (Typical Meteorological Year) weather files, providing hourly temperature, humidity, wind speed, and solar radiation data. The UTCI calculation methodology follows established protocols (Bröde et al., 2012):

$$UTCI = T_{air} + \Delta T_{UTCI} \tag{3}$$

where T_{air} represents air temperature and ΔT_{UTCI} represents the offset calculated from wind speed, mean radiant temperature, and relative humidity using the UTCI polynomial approximation. Mean radiant temperature calculations incorporate solar radiation, surface temperatures, and view factors between human subjects and surrounding surfaces.

The implementation of MRT calculation in this study follows a multi-step approach integrating solar radiation modeling, surface temperature calculation, and view factor analysis. Solar radiation modeling utilizes the Perez all-weather sky model implemented in Ladybug Tools (Perez et al., 1988), processing hourly solar radiation data from Shenzhen TMY weather files. The solar radiation incident on each surface element considers direct normal irradiance with sun position calculations using astronomical algorithms for Shenzhen's coordinates (22.55°N, 114.07°E), diffuse horizontal irradiance distributed according to the Perez sky luminance model, and ground-reflected radiation with albedo values of 0.2 for asphalt surfaces and 0.25 for concrete.

Building surface temperatures are derived from solar heat gain analysis combined with surface material thermal properties. For each surface element, the surface temperature is calculated as:

$$T_{surf} = T_{air} + \frac{I_{solar} \times \alpha}{h_c + h_r} \tag{4}$$

where I_{solar} is total solar irradiance on the surface, α is solar absorptance (0.7 for concrete, 0.9 for dark surfaces), h_c is convective heat transfer coefficient, and h_r is radiative heat transfer coefficient. The geometric relationship between human subjects and surrounding surfaces is quantified through view factor calculations using hemisphere projection methods. The study implements a discretized approach where the hemisphere above each calculation point is divided into a regular grid of 145 sky patches following the Tregenza sky discretization (Tregenza, 2004). Ray-tracing algorithms determine surface visibility for each sky patch direction, with view factors calculated using the projected solid angle method:

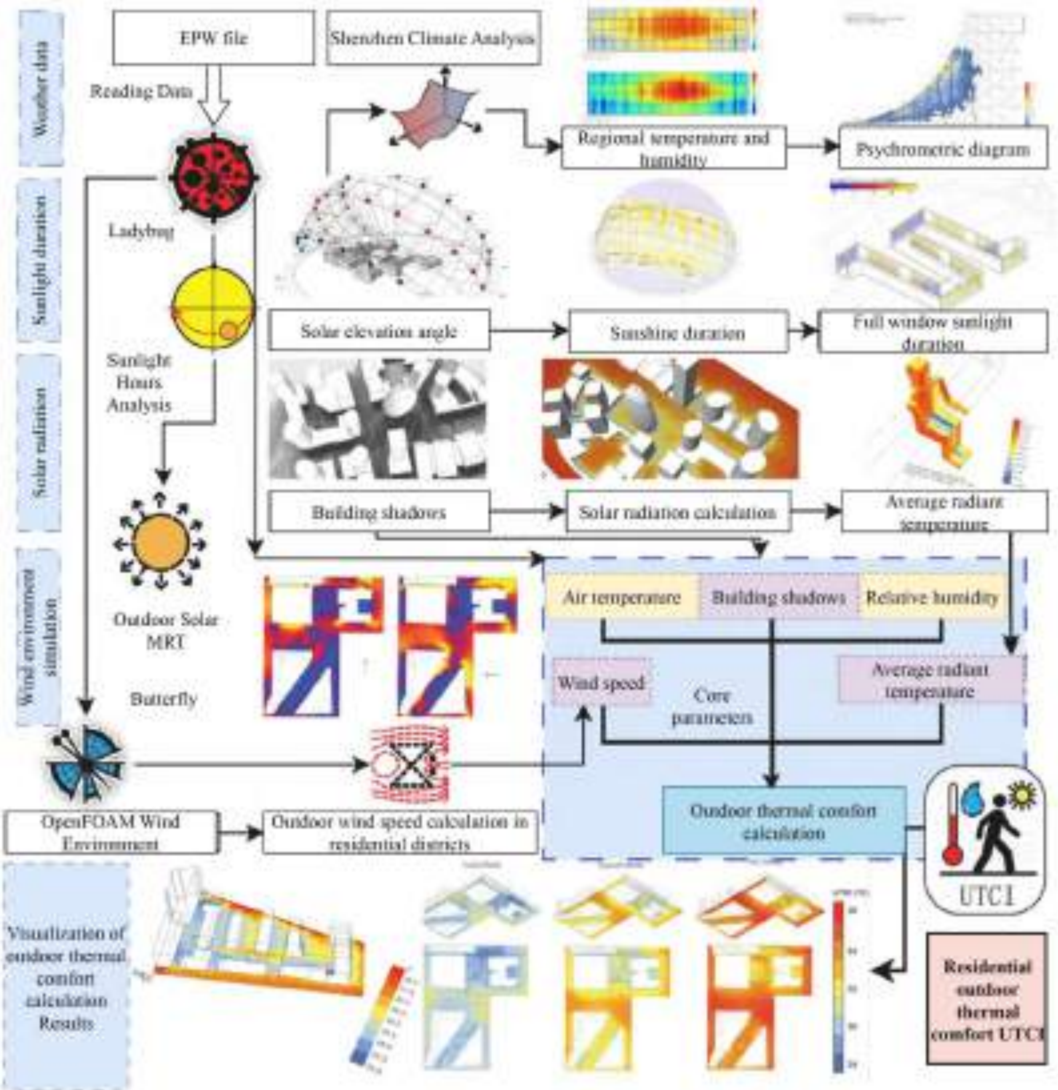

Fig. 7. Environmental performance simulation workflow.

$$F_{i-j} = \frac{1}{\pi} \int \int \frac{\cos\theta_i \times \cos\theta_j}{\pi r^2} dA_i dA_j \tag{5}$$

where θ_i and θ_j are angles between surface normals and the connecting line, and r is the distance between surface elements.

The final MRT calculation integrates radiative contributions from all visible surfaces:

$$T_{mrt} = \left[\sum \left(F_i \times T_{surf,i}^4 \right) \right]^{1/4} \tag{6}$$

where F_i is the view factor to surface i, and $T_{surf,i}$ is the temperature of surface i in Kelvin. The MRT calculation process is automated through Grasshopper's Honeybee Radiance and Ladybug components, with custom Python scripts handling view factor calculations and surface temperature analysis. The computational grid employs 1 m × 1 m resolution at 1.5 m height to represent pedestrian-level conditions. The simulation focuses on critical summer weeks, typically late July when thermal stress is maximum, with additional winter solstice analysis for daylighting compliance verification.

3.5.2. CFD simulation and wind environment

Wind environment simulation employs the Butterfly plugin interfacing with OpenFOAM CFD solver, enabling high-fidelity airflow predictions around building configurations (Dogan and Kastner, 2021). The computational approach utilizes steady-state RANS equations with k-ε turbulence closure, appropriate for urban-scale wind environment assessment. Computational domains extend 5H upstream, 15H downstream, and 5H laterally from building groups, with top boundaries at 6H to minimize blockage effects. Mesh generation employs structured hexahedral grids with local refinement near building surfaces and in wake regions where flow gradients are significant.

Boundary conditions specify representing urban boundary layer characteristics (Tennekes, 1973):

$$U(z) = \frac{u_*}{\kappa}\ln\left(\frac{z}{z_0}\right) \tag{7}$$

where u_* is friction velocity, κ is the von Kármán constant (0.41), z is height above ground, and z_0 is surface roughness length. The surface roughness length was set to $z_0 = 2$ m, representing Shenzhen's center city with medium development density that is typical for Shenzhen's residential areas according to the terrain classification. Reference wind speeds correspond to typical summer conditions in Shenzhen based on weather station data analysis.

3.5.3. Daylighting analysis and building code compliance

Daylighting analysis targets winter solstice compliance with Chinese residential building standards, requiring minimum 1-h direct sunlight exposure for primary living spaces between 9:00–15:00. The simulation employs ray-tracing algorithms to calculate solar exposure duration on building facades, accounting for inter-building shadowing and seasonal sun path variations. Solar position calculations utilize standard astronomical algorithms corrected for Shenzhen's geographic coordinates (22.55°N, 114.07°E).

The integrated simulation workflow processes parametric building configurations through parallel analysis streams, generating thermal comfort, wind speed, and daylighting duration maps for each candidate design. Results are aggregated into scalar performance metrics suitable for optimization algorithms, including area-weighted average UTCI values across pedestrian zones, minimum wind speeds for natural ventilation, and daylighting compliance percentages.

3.6. Multi-objective optimization algorithm

The optimization framework employs genetic algorithm methodology implemented through the Wallacei plugin, specifically designed for architectural applications requiring simultaneous consideration of multiple conflicting objectives (Zaker Vafaee et al., 2022). The algorithm targets dual objectives: minimizing summer thermal discomfort (expressed as UTCI reduction) and maximizing winter daylighting performance (expressed as facade-averaged solar exposure duration).

The genetic algorithm utilizes real value encoding to represent continuous design variables including building dimensions, positions, and orientations. Population initialization employs Latin Hypercube Sampling to ensure uniform coverage of the design space, with initial population size set to 100 individuals based on convergence analysis. Selection mechanisms combine tournament selection for parent choice with elitist preservation to maintain high-quality solutions across generations.

Crossover and mutation operators are specifically adapted for architectural design variables. Simulated Binary Crossover (SBX) handles continuous parameters with distribution index η = 15 to balance exploration and exploitation. Polynomial mutation provides bounded perturbations with probability 1/n (where n equals the number of variables) and distribution index η = 20. The multi-objective optimization employs the NSGA-II algorithm for Pareto frontier identification:

Table 5
Summary of residential neighborhood database characteristics.

Building Type	Building Density Distribution	Peak Density Range (%)	FAR Range	Peak FAR Range	Building Width (m)	Building Depth (m)	Orientation Preference
Multi-story (4–9 floors)							
Row-style	21–35%	27–28%	1.1–2.7	<2.5	40–65	12–24	South ±15°
Cluster-style	21–35%	27–28%	1.1–2.7	<2.5	20–50	20–50	South ±30°
Courtyard-style	21–35%	27–28%	1.1–2.7	<2.5	25–65	10–30	South ±10°
High-rise Type II (10–18 floors)							
Row-style	16–28%	20–25%	1.4–3.4	2.0–3.0	40–65	12–24	South ±15°
Cluster-style	16–28%	20–25%	1.4–3.4	2.0–3.0	20–50	20–50	South ±30°
Courtyard-style	16–28%	20–25%	1.4–3.4	2.0–3.0	25–65	10–30	South ±10°
High-rise Type I (19–33 floors)							
Row-style	11–25%	15–20%	2.4–6.0	2.4–2.8	40–65	12–24	South ±15°
Cluster-style	11–25%	15–20%	2.4–6.0	2.4–2.8	20–50	20–50	South ±30°
Courtyard-style	11–25%	15–20%	2.4–6.0	2.4–2.8	25–65	10–30	South ±10°

Note: Data derived from comprehensive survey of 972 residential neighborhoods across Shenzhen's four central districts (Futian, Luohu, Nanshan, and Bao'an), with detailed morphological analysis of 164 representative cases encompassing 2031 individual buildings. FAR = Floor Area Ratio. Orientation preferences indicate typical angular deviation from due south orientation.

$$\text{Minimize}: f_1(x) = \overline{UTCI_{summer}} \tag{8}$$

$$\text{Maximize}: f_2(x) = \overline{t_{daylight,winter}} \tag{9}$$

Subject to constraints:

- Building density $\leq$ maximum allowable per classification
- Floor area ratio within specified ranges
- Minimum building separation distances
- Winter solstice daylighting compliance
- Fire access requirements

The optimization process continues for 50 generations based on convergence analysis, generating approximately 3000 evaluated configurations per layout typology. Pareto frontier solutions represent optimal trade-offs between thermal comfort and daylighting objectives, providing designers with multiple high-performance alternatives suitable for different project priorities and constraints.

4. Results and analysis

4.1. Residential neighborhood database characteristics

The comprehensive survey of 972 residential neighborhoods across Shenzhen's four central districts revealed distinct morphological patterns that inform parametric modeling constraints, as summarized in Table 5. Statistical analysis demonstrates significant variations in building density and floor area ratio (FAR) distributions across different building height classifications, reflecting evolving urban planning policies and market demands over the past two decades.

Multi-story residential neighborhoods (4–9 floors) exhibit remarkably consistent characteristics across all layout types, with building densities concentrated between 21 and 35% and peak occurrence at 27–28%. The FAR distribution ranges from 1.1 to 2.7, with most developments clustering below 2.5, indicating conservative density approaches that prioritize open space and natural lighting. This consistency suggests standardized planning approaches for low-rise developments regardless of spatial arrangement strategy. High-rise Type II districts (10–18 floors) demonstrate increased development flexibility, with building densities reduced to 16–28% ranges and peak concentrations between 20 and 25%. FAR distributions show greater variation, spanning 1.4 to 3.4 with peak ranges of 2.0–3.0, reflecting the enhanced design flexibility enabled by vertical development strategies. This broader range indicates more diverse market responses and planning adaptations for medium-height developments. High-rise Type I developments (19–33 floors) exhibit the most intensive land use patterns, with FAR values ranging from 2.4 to 6.0 and peak concentrations between 2.4 and 2.8. Building densities are correspondingly reduced to 11–25% with peak ranges of 15–20%, demonstrating the inverse relationship between building height and site coverage. These patterns confirm theoretical expectations that vertical intensification enables reduced ground coverage while achieving high development densities.

Morphological parameter analysis reveals layout-specific dimensional characteristics that reflect functional optimization strategies. Row-style configurations consistently feature the largest building widths (40–65 m) with moderate depths (12–24 m) across all building heights, reflecting optimization for natural lighting and cross-ventilation in linear arrangements. Cluster-style layouts exhibit the most balanced width-depth relationships (20–50 m in both dimensions), supporting point-building configurations that maximize spatial openness and view access. Courtyard-style developments show the greatest dimensional variation, with widths spanning 25–65 m and depths ranging 10–30 m, accommodating diverse enclosure strategies from intimate courtyards to large communal spaces.

Building orientation analysis demonstrates layout-dependent preferences that reflect both climatic optimization and urban fabric integration constraints. Row-style layouts show the most concentrated orientation distribution (south $\pm 15^\circ$), indicating strong climate-responsive design practices that prioritize solar access and natural ventilation. Cluster-style configurations exhibit greater angular dispersion (south $\pm 30^\circ$), reflecting increased flexibility in point-building arrangements that can accommodate varied site conditions. Courtyard-style developments demonstrate the narrowest orientation range (south $\pm 10^\circ$) due to perimeter alignment requirements and the need to optimize internal courtyard solar access.

The database characteristics reveal clear relationships between building height, development density, and morphological flexibility. Lower buildings maintain higher site coverage but show less dimensional variation, while taller developments achieve greater FAR through reduced coverage and increased morphological diversity. These empirical patterns provide robust foundations for parametric modeling constraints and validation of optimization outcomes against real-world development practices.

4.2. Numerical model validation results

4.2.1. Validation of the ideal neighborhood model

The validation employed AIJ standard test cases for isolated building configurations, providing benchmark scenarios with known experimental results for systematic assessment of CFD model performance under controlled conditions. The validation examined three wind incidence angles (0°, 22.5°, and 45°) using progressively refined mesh resolutions as indicated in AIJ Case C, and the results are shown in Figure X. For the 0° wind angle case, the coarse mesh (Index of Agreement (IoA) = 0.75, RMSE = 0.16) showed acceptable but limited accuracy in capturing the experimental velocity distribution. The medium mesh configuration (IoA = 0.73, RMSE = 0.17) demonstrated comparably better performance than the coarse mesh, while the fine mesh (IoA = 0.83, RMSE = 0.12) achieved significantly improved agreement with experimental data, particularly in resolving wake regions and building-induced flow separations as shown in Fig. 8.

At 22.5° wind incidence, mesh configurations showed enhanced prediction accuracy with the growing mesh quality. The coarse mesh achieved IoA = 0.76 with RMSE = 0.18, the medium mesh reached IoA = 0.81 with RMSE = 0.16, and the fine mesh demonstrated superior performance with IoA = 0.84 and RMSE = 0.13. The improved correlations at this angle suggest better numerical stability in capturing oblique flow patterns around building geometries. The 45° wind angle case presented the most challenging validation scenario, with increased flow complexity due to pronounced asymmetric wake development. The coarse mesh (IoA = 0.78, RMSE = 0.19) maintained reasonable accuracy despite the complex flow field. The medium mesh (IoA = 0.81, RMSE = 0.16) showed marked improvement, while the fine mesh configuration (IoA = 0.87, RMSE = 0.13) achieved the highest validation metrics across all tested conditions.

The spatial bias distribution plots reveal systematic patterns in model performance. All mesh resolutions consistently captured the upstream flow field with minimal bias, while downstream regions exhibited mesh-dependent variations. The coarse mesh showed positive bias (overestimation) in the near-wake region, particularly evident at X = 0.1–0.2 m downstream of the building. The medium mesh reduced this systematic bias, though localized discrepancies persisted in regions of strong flow gradients. The fine mesh configuration minimized both systematic and random errors, demonstrating superior capability in resolving complex urban flow features critical for thermal comfort assessment.

The validation results confirm that the fine mesh configuration achieves IoA values around 0.83 across all wind angles, surpassing the AIJ-recommended threshold of 0.8 for urban CFD applications. The consistent RMSE values also demonstrate acceptable absolute error magnitudes for subsequent optimization studies. Based on these validation metrics, the fine mesh resolution was selected for all subsequent parametric optimization analyses to ensure reliable thermal comfort predictions while maintaining computational feasibility for large-scale optimization investigations.

4.2.2. Field measurement and validation

Field validation using meteorological stations deployed in Bao'an district provided additional confidence in model reliability under actual urban conditions. Two micro-environmental monitoring stations were strategically positioned to capture different urban microclimate characteristics during typical summer conditions.

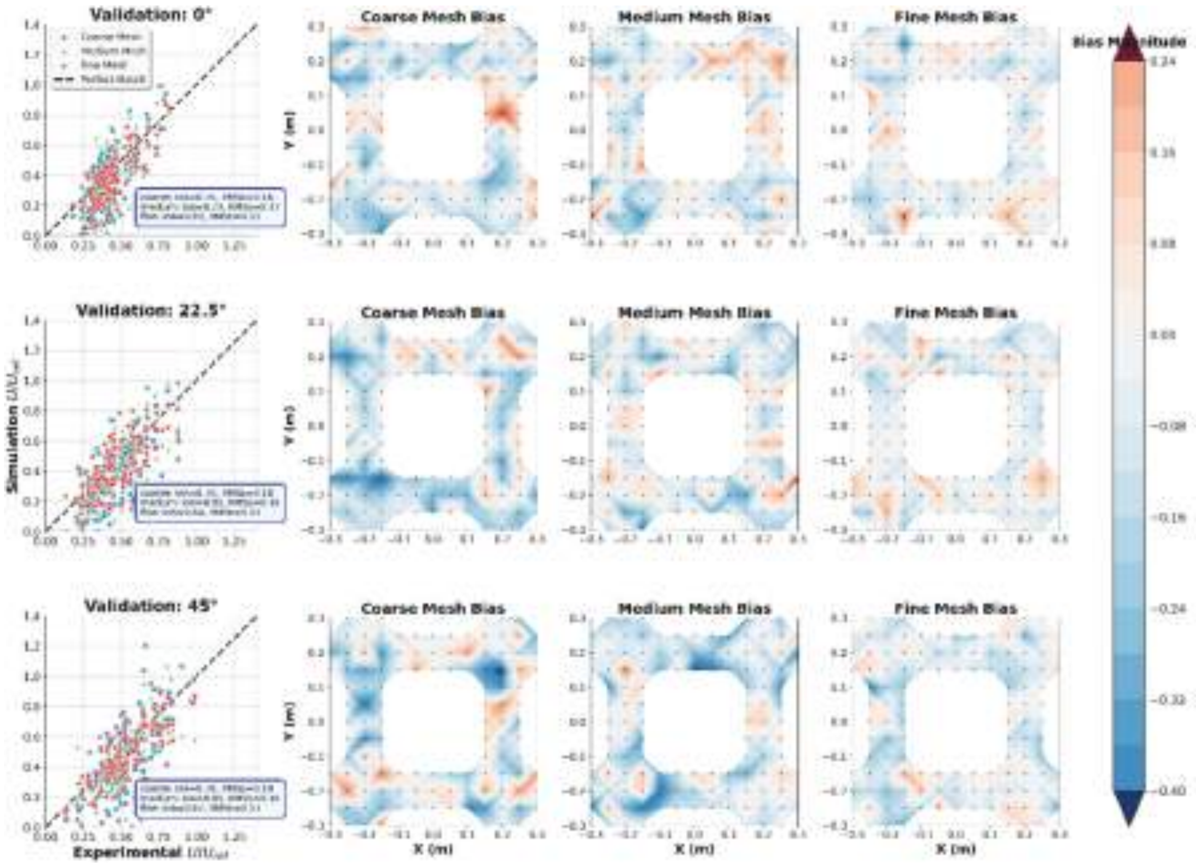

Fig. 8. CFD validation vs. AIJ case C: simulation bias and correlation analysis.

Fig. 9 presents time-series comparisons between simulated and measured wind speeds at both monitoring locations. Station 1, located near Baosheng Hospital within a green corridor, represents a semi-open urban environment with moderate building density. The measurement campaign recorded wind speeds ranging 0.8–2.1 m/s with good agreement between measured and simulated values (RMSE = 0.253 m/s, d = 0.79). Station 2, positioned in the central pedestrian area of Anle Garden residential complex, characterizes higher building density and more enclosed spatial conditions. This location showed lower wind speeds (0.6–1.8 m/s) with slightly better simulation accuracy (RMSE = 0.145 m/s, d = 0.70).

The field validation results confirm that the coupled simulation framework can capture wind flow patterns around building configurations typical of Shenzhen's residential neighborhoods. Both monitoring stations achieved consistency indices approaching 0.8, demonstrating acceptable model performance for urban design applications. The slightly lower consistency values compared to controlled AIJ validation reflect the inherent complexity of real urban environments, where atmospheric stability variations, local topographic effects, and temporal meteorological fluctuations introduce additional uncertainty not captured in steady-state simulations.

Controlled discrepancies between measured and simulated values can be attributed to several factors including temporal variations in atmospheric stability, local microclimatic effects from vegetation and surface materials, and measurement uncertainties associated with urban wind monitoring. The RMSE values below 0.26 m/s for both stations fall within acceptable tolerances for urban CFD applications, confirming model reliability for residential neighborhood optimization studies.

4.3. Multi-objective optimization results

Genetic algorithm optimization across 30 generations successfully identified Pareto optimal solutions balancing thermal comfort and daylighting objectives for all nine experimental configurations (three layout types × three building height categories). Convergence analysis demonstrates progressive improvement in objective function values with stabilization occurring around generation 20–25, confirming adequate evolution duration.

Multi-story residential neighborhoods achieved the most favorable optimization outcomes across all layout types. Row-style configurations demonstrated superior convergence characteristics, with UTCI values decreasing from initial ranges of 32.0–32.5 °C to optimized values of 31.6–31.8 °C, as shown in Fig. 10 (a-b). Winter solstice daylighting performance simultaneously improved from 1.8 to 2.2 h to stabilized ranges of 2.3–2.5 h. Cluster-style layouts achieved comparable thermal comfort improvements (UTCI reduction of 0.4–0.6 °C) while maintaining consistently high daylighting performance above 2.5 h throughout optimization, as illustrated in Fig. 10 (c-d). Courtyard-style configurations showed more modest improvements in both objectives, with final UTCI values of 31.8–32.0 °C and daylighting durations of 2.39–2.45 h, as presented in Fig. 10 (e-f).

High-rise Type II developments exhibited layout-dependent optimization patterns. Row-style arrangements achieved UTCI improvements from 32.4 to 32.6 °C to 32.27–32.35 °C, with daylighting enhancement from 2.25 to 2.42 h to 2.48–2.5 h. The convergence process is shown in Fig. 11 (a-b). Cluster-style configurations demonstrated superior thermal comfort optimization, reaching final UTCI values of 32.2–32.65 °C while maintaining daylighting performance of 2.25–2.5 h, as illustrated in Fig. 11 (c-d). Courtyard-style layouts showed the most dramatic improvements, with UTCI reductions from 32.95 to 32.8 °C to 32.7–33.1 °C, though absolute performance remained inferior to other layout types. These results are presented in Fig. 11 (e-f).

High-rise Type I districts presented the greatest optimization challenges due to increased building mass and reduced inter-building spacing. Row-style layouts achieved substantial UTCI improvements from initial values of 34.2–32.8 °C to optimized ranges of 32.5–33.48 °C, representing the largest absolute thermal comfort gains. The optimization convergence is shown in Fig. 12 (a-b). Cluster-style configurations demonstrated more consistent performance across both objectives, with final UTCI values of 32.35–32.7 °C and daylighting durations of 2.38–2.41 h, as illustrated in Fig. 12 (c-d). Courtyard-style developments showed limited optimization potential, with final UTCI values remaining above 33.0 °C despite modest improvements. These results are presented in Fig. 12 (e-f).

Wind speed analysis reveals layout-specific patterns influencing thermal comfort outcomes, as shown in Fig. 13. Cluster-style configurations consistently achieve the highest wind speeds (1.5–2.5 m/s), supporting natural ventilation and evaporative cooling.

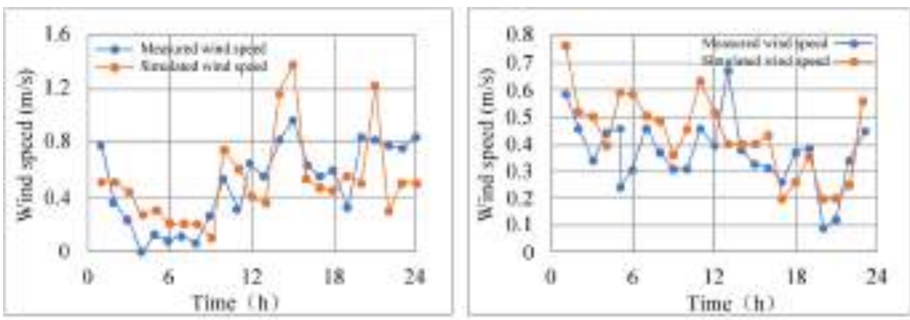

(a) Measurement station 1: Baosheng Hospital (b) Measurement station 2: Anle Garden

Fig. 9. Comparison of onsite measured and simulated wind speeds.

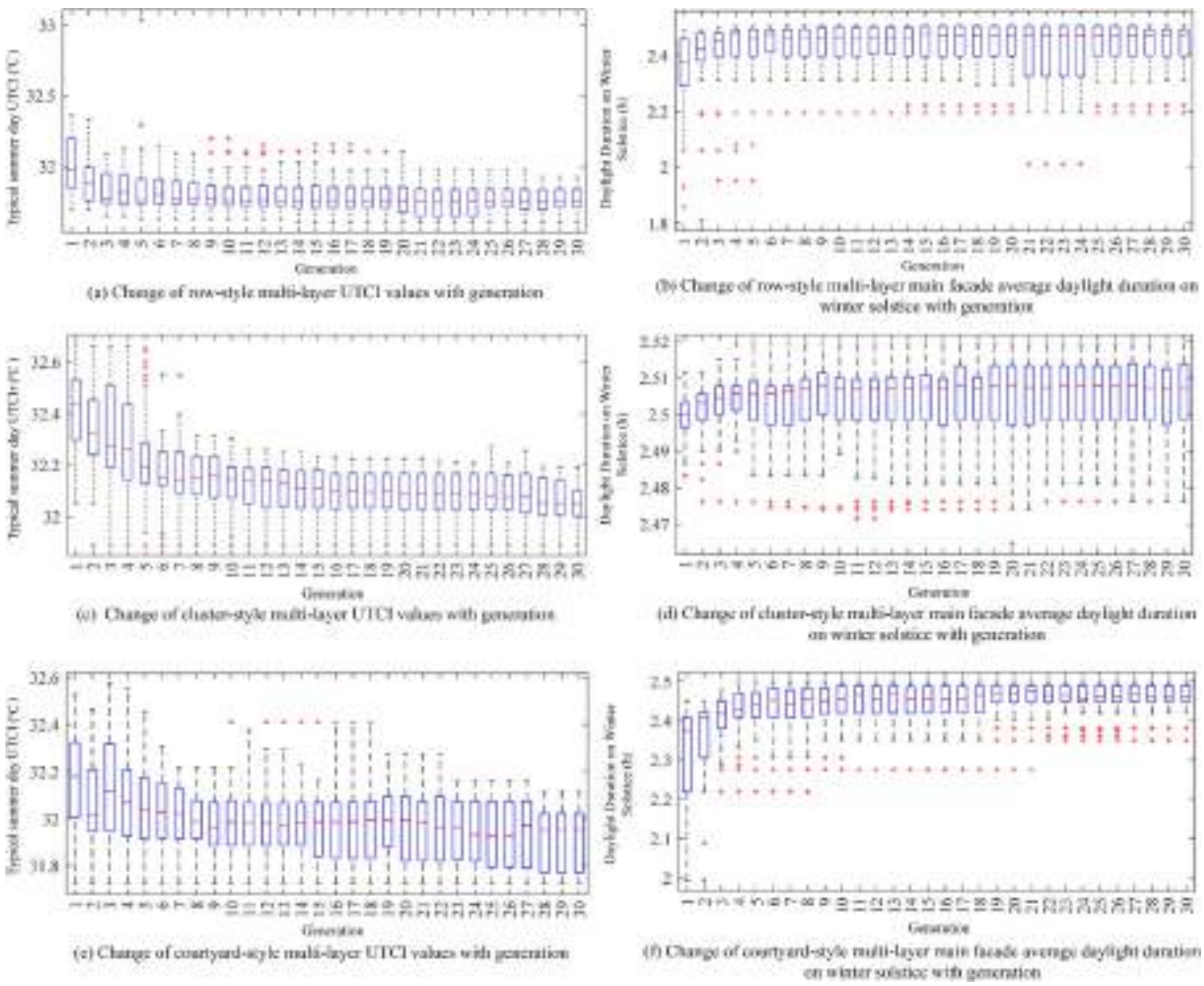

Fig. 10. Convergence process of multi-story residential neighborhood optimization.

Row-style layouts demonstrate intermediate wind speeds (1.0–2.2 m/s) with height-dependent variations. Courtyard-style arrangements exhibit the lowest wind speeds (1.2–1.8 m/s), contributing to thermal comfort limitations despite beneficial shading effects.

The Pareto frontiers generated from the multi-objective optimization are presented in Fig. 14, illustrating the trade-off relationships between summer thermal comfort and winter solstice daylighting performance. The optimization direction indicated by arrows in Fig. 14(a) and (b) emphasizes that ideal solutions should minimize summer UTCI while maximizing winter daylighting duration, with solutions positioned in the upper-left region of each plot representing superior multi-objective performance. For multi-story configurations shown in Fig. 14(a), row-style layouts achieved the most favorable Pareto frontier position with optimal solutions extending toward lower UTCI values while maintaining daylighting durations above 2.4 h, whereas cluster-style and courtyard-style configurations exhibited more compact Pareto distributions concentrated around moderate performance levels. In high-rise Type II developments shown in Fig. 14(b), all three layout types demonstrated broader solution distributions with courtyard-style configurations showing the widest spread in daylighting performance, indicating greater sensitivity to morphological parameter variations. For high-rise Type I configurations shown in Fig. 14(c), the Pareto frontiers shifted toward higher UTCI values reflecting increased thermal challenges associated with taller building masses, with row-style layouts maintaining relatively compact high-performing solution clusters while courtyard-style configurations exhibited the most dispersed distribution extending to lower daylighting values.

4.4. Morphological parameter impact quantification

Regression analysis quantified relationships between design parameters and environmental performance indicators, revealing layout-specific sensitivity patterns critical for design optimization. Building density effects demonstrate significant layout dependency, with correlation coefficients ranging from negligible to strong depending on building type and arrangement configuration.

For thermal comfort optimization, building density shows contrasting effects across layout types. As shown in Fig. 15, for high-rise Type II configurations, row-style developments demonstrate moderate positive correlation between building density and UTCI ($R^2 =$

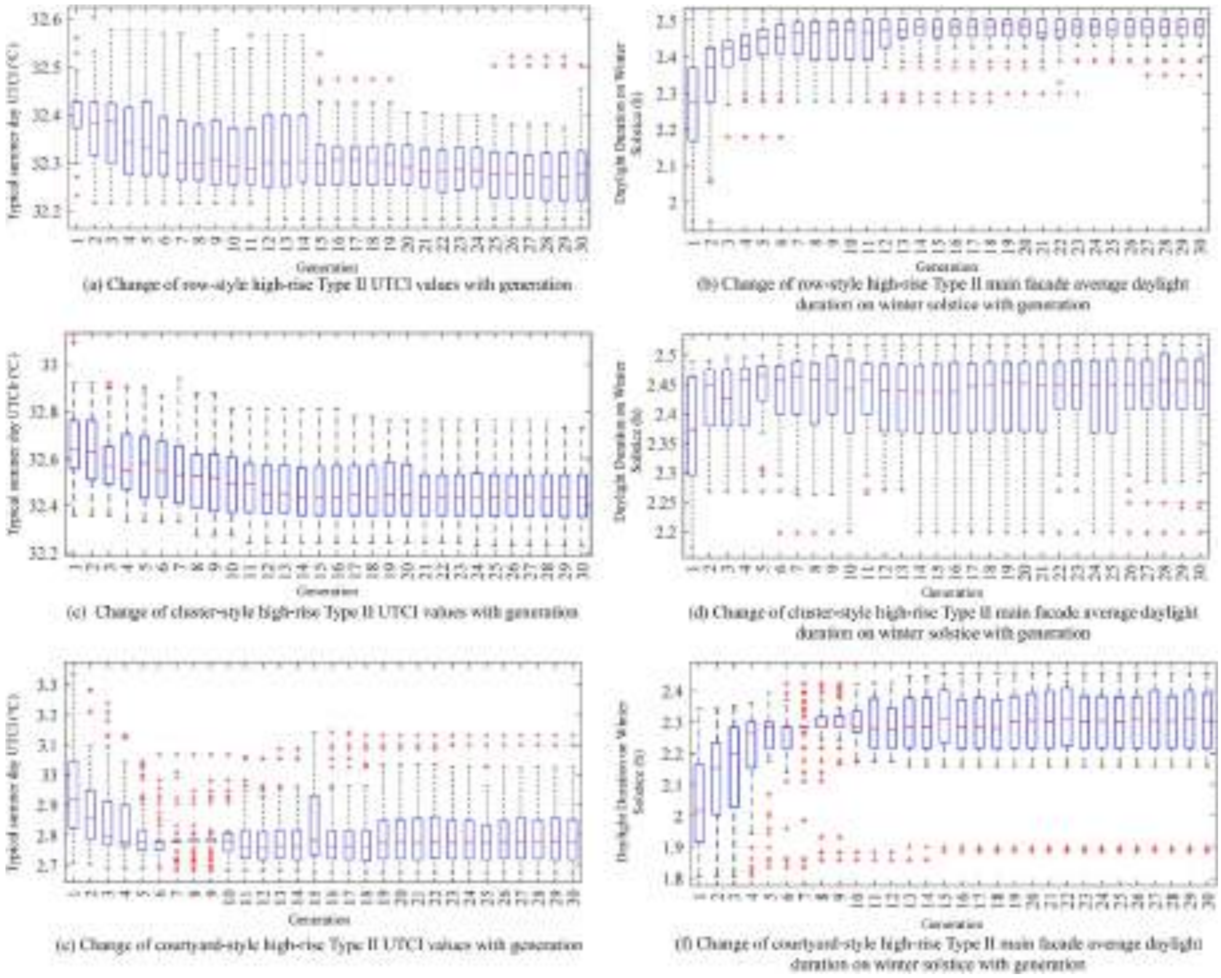

Fig. 11. Optimization convergence process of high-rise Type II residential neighborhoods.

0.49856), indicating thermal comfort degradation with increased density. Conversely, cluster-style layouts show moderate negative correlation ($R^2 = 0.55973$), suggesting that increased density can improve thermal comfort through enhanced shading effects. Courtyard-style developments demonstrate the strongest density-thermal comfort correlation among the three layout types ($R^2 = 0.6252$), also exhibiting a negative relationship where higher density contributes to lower UTCI values. Regarding daylighting performance, all three layout types show weak correlations between building density and winter solstice sunlight duration, with courtyard-style configurations demonstrating the highest sensitivity ($R^2 = 0.28451$), followed by cluster-style ($R^2 = 0.16727$) and row-style ($R^2 = 0.13639$) layouts.

As shown in the Table 6, floor area ratio (FAR) impacts follow similar layout-dependent patterns but with generally stronger correlations. Cluster-style high-rise developments show the most pronounced FAR-thermal comfort relationships, with R^2 values exceeding 0.8 for Type II configurations. Row-style layouts demonstrate moderate FAR sensitivity in high-rise Type I developments ($R^2 = 0.328$), while courtyard-style configurations exhibit strong correlations across all building heights.

Morphological parameters including width-depth ratio, building width, depth, height-width ratio, rotation angle, and floor count show varying influence depending on layout type and building height. Cluster-style configurations demonstrate the strongest parameter sensitivity, with building width showing significant negative correlation with UTCI in high-rise developments ($R^2 = 0.354$ for Type II, $R^2 = 0.414$ for Type I). Building depth correlates negatively with thermal comfort across all cluster-style configurations, with correlation strength increasing with building height. Height-width ratio effects are most pronounced in courtyard-style layouts, where increased ratios consistently improve thermal comfort through enhanced shading. Row-style configurations show weaker height-width ratio correlations, while cluster-style layouts demonstrate minimal sensitivity to this parameter.

Building rotation angle impacts vary significantly across layout types and building heights. Row-style multi-story developments show weak negative correlation with UTCI, while high-rise Type I configurations in both row-style and cluster-style layouts demonstrate positive correlations, suggesting increased thermal stress with eastward rotations. Courtyard-style high-rise Type I developments show negative correlation with rotation angle, indicating thermal comfort benefits from eastward orientation adjustments.

Floor count relationships reveal consistent patterns across layout types, with negative correlations indicating thermal comfort

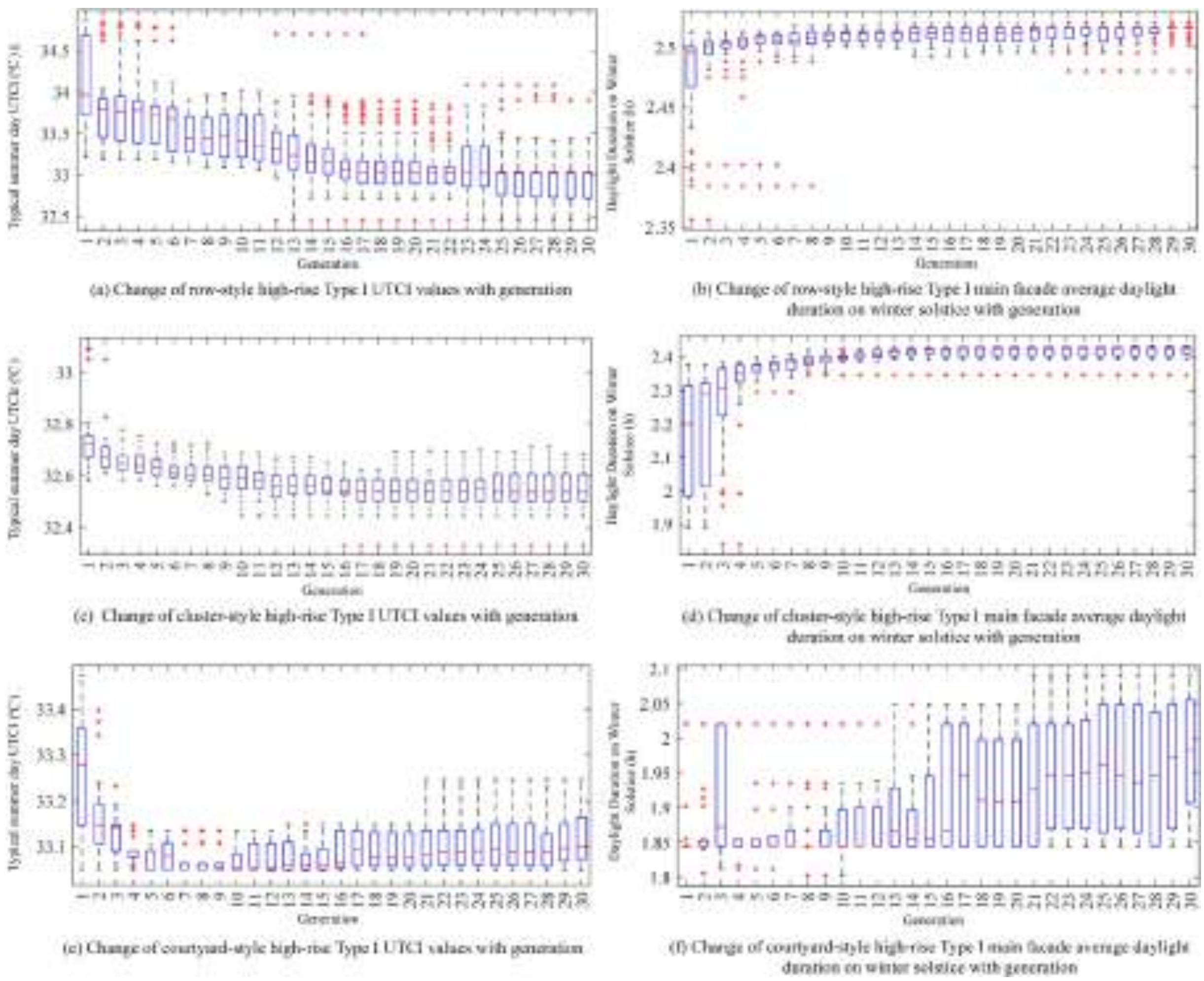

Fig. 12. Optimization convergence process of high-rise Type I residential neighborhoods.

improvements through increased building height when development density remains constant. Courtyard-style configurations show the strongest floor count effects (R^2 = 0.502–0.602), while cluster-style developments demonstrate moderate correlations (R^2 = 0.257–0.426).

4.5. Practical application for residential renewal

The Bao'an district renewal project provided validation of optimization methodology under real-world constraints. The 180 m × 140 m redevelopment site, surrounded by existing multi-story buildings and one high-rise structure, presented typical urban infill challenges requiring careful balance between development intensity and environmental performance.

Pre-optimization thermal environment analysis revealed average UTCI values of 32.7 °C across the site during typical summer weeks, with localized hot spots exceeding 34 °C in areas with poor ventilation and excessive solar exposure. The existing urban fabric created wind shadow effects reducing natural ventilation and contributing to thermal comfort degradation. Application of regression analysis findings to parameter adjustment strategies yielded measurable performance improvements across all layout configurations. Table 7 shows the improvement of performance after optimization for different neighborhood layouts. Row-style arrangements achieved UTCI reductions of 0.2–0.6 °C through optimized building spacing and orientation adjustments. Cluster-style configurations demonstrated UTCI improvements of 0.45 °C via strategic density increases and morphological parameter optimization. Courtyard-style layouts achieved 0.4 °C thermal comfort improvements through dispersed arrangement strategies and selective open space integration.

The optimization process successfully generated feasible design solutions meeting regulatory requirements while achieving substantial environmental performance improvements. Winter solstice daylighting compliance was maintained across all configurations, with enhanced thermal comfort representing net environmental benefit without compromising basic habitability standards.

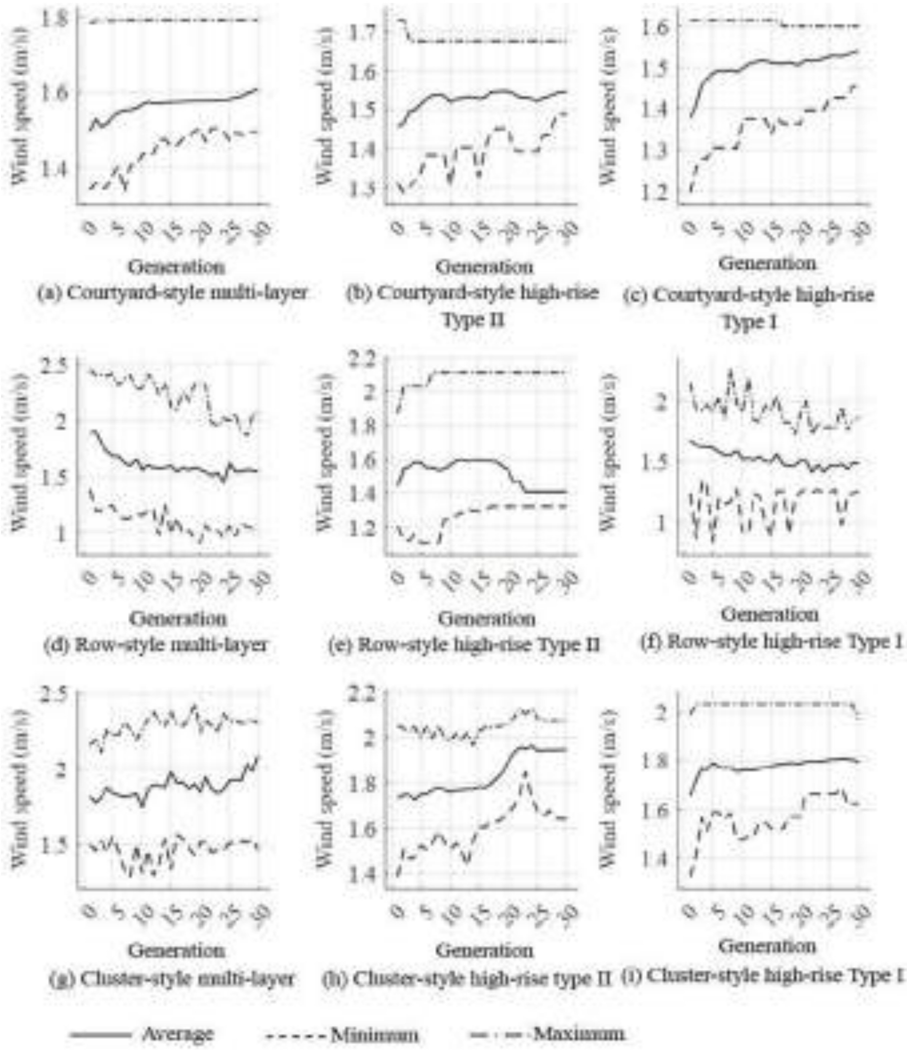

Fig. 13. Changes in outdoor average wind speed during residential neighborhood optimization.

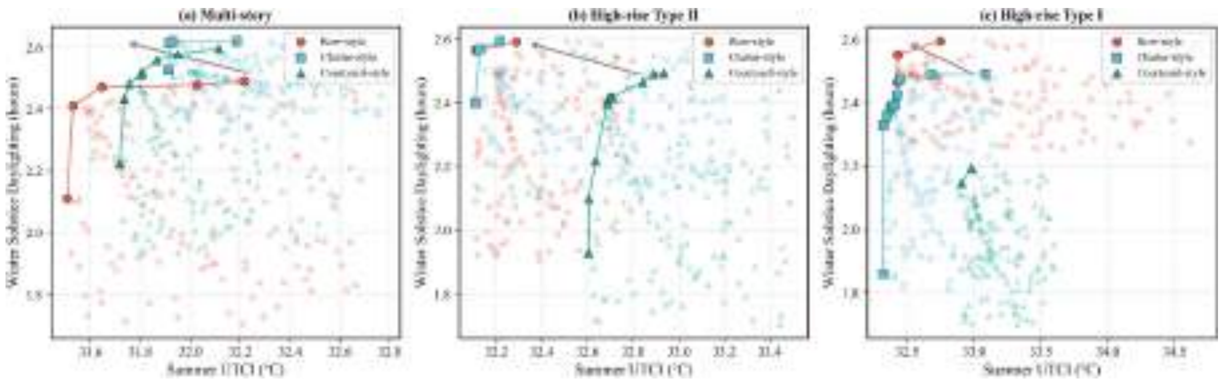

Fig. 14. Pareto frontiers showing trade-offs between summer UTCI and winter solstice daylighting duration for different residential neighborhoods.

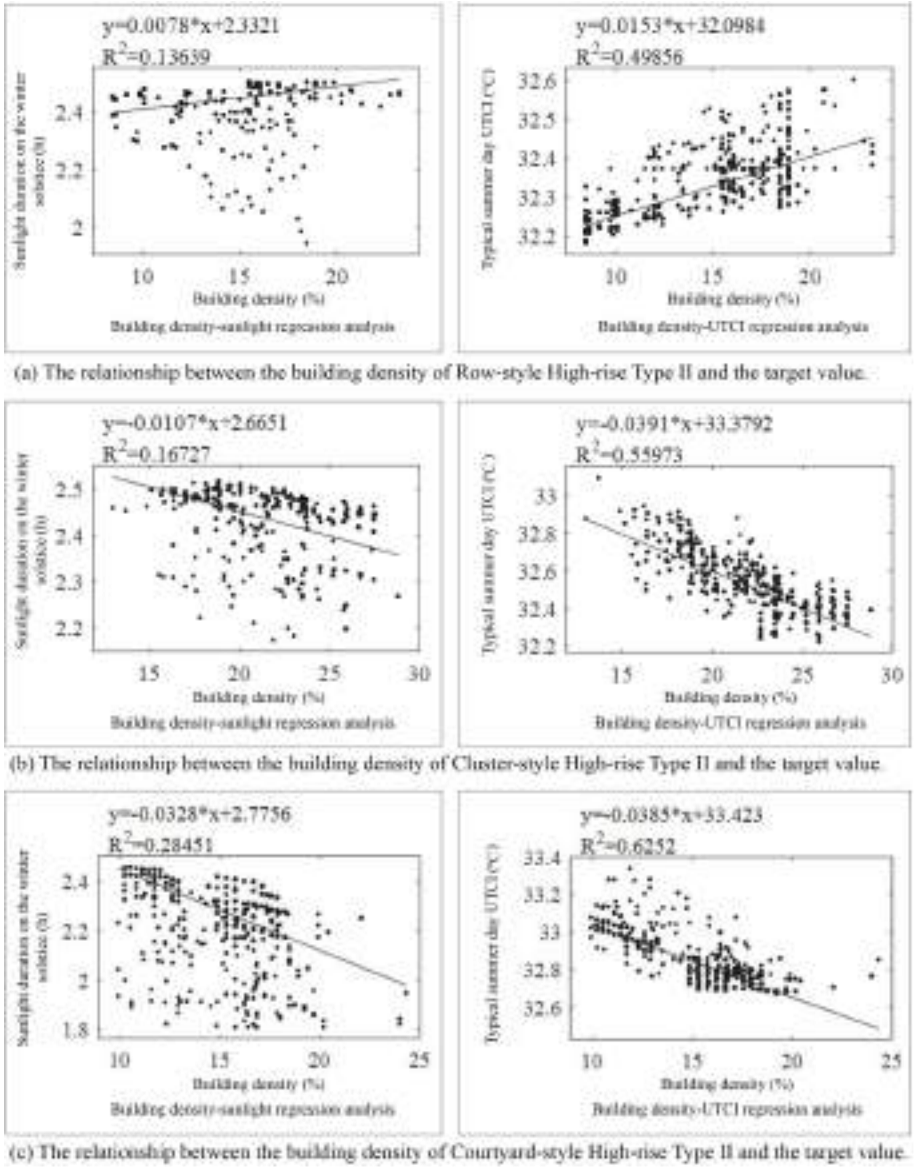

Fig. 15. Regression analysis of relationships between design parameters and environmental performance indicators.

4.6. *Design optimization application using case study*

The case study renewal project in Bao'an district served as a testbed for the parametric optimization methodology under real-world urban constraints. The 180 m × 140 m redevelopment site, situated within Shenzhen's established urban fabric, presented typical challenges for high-density residential development while maintaining environmental performance standards as shown in Fig. 16.

Initial thermal environment assessment revealed significant comfort deficiencies across the development site. The existing urban configuration generated average UTCI values of 32.7 °C during typical summer conditions, with localized hot spots exceeding 34 °C in areas experiencing poor natural ventilation and excessive solar exposure. The surrounding building arrangement created wind shadow effects that substantially reduced airflow across the site, contributing to thermal stagnation and heat accumulation. These baseline conditions provided clear performance improvement targets for the optimization process.

4.6.1. *Parameter adjustment strategy implementation*

Based on the regression analysis findings detailed in Section 4.4, systematic parameter adjustments were implemented across all nine layout-building height combinations. The adjustment strategy prioritized parameters demonstrating strong correlations with thermal comfort performance while maintaining regulatory compliance and development feasibility.

For row-style configurations, building density reductions of 5% were applied to high-rise Type II developments due to their positive

Table 6
Correlation summary of neighborhood morphological parameter impact on thermal comfort.

Parameter	Row-style			Cluster-style			Courtyard-style		
	Multi	HR-II	HR-I	Multi	HR-II	HR-I	Multi	HR-II	HR-I
Building Density	0	++	–	–	–	–	0	–	–
Floor Area Ratio	–	–	–	–	–	–	–	–	–
Width-Depth Ratio	0	–	+	0	0	0	–	++	+
Building Width	0	–	+	0	–	–	0	0	–
Building Depth	0	+	0	–	–	–	0	–	–
Height-Width Ratio	0	–	–	0	0	0	–	–	–
Rotation Angle	–	0	+	0	0	+	0	0	–
Building Floors	0	–	0	–	–	–	–	–	–

Note:
0: No correlation ($R^2 < 0.1$)
+/−: Weak correlation ($0.1 \leq R^2 < 0.4$) - Positive/Negative
++/−−: Moderate correlation ($0.4 \leq R^2 < 0.7$) - Positive/Negative
+++/−−-: Strong correlation ($R^2 \geq 0.7$) - Positive/Negative
Multi: Multi-story (4–9 floors)
HR-II: High-rise Type II (10–18 floors)
HR-I: High-rise Type I (19–33 floors)

Table 7
Residential neighborhood model performance comparison.

Layout Type	Building Type	Thermal Comfort Optimal Model (UTCI °C)	Thermal Comfort Worst Model (UTCI °C)	Performance Improvement (°C)
Row-style	Multi-story	31.84	32.42	0.58
	High-rise Type II	32.34	32.85	0.51
	High-rise Type I	32.9	33.25	0.35
Cluster-style	Multi-story	31.66	32.19	0.53
	High-rise Type II	32.24	32.7	0.46
	High-rise Type I	32.6	32.98	0.38
Courtyard-style	Multi-story	32.35	32.6	0.25
	High-rise Type II	32.62	32.9	0.28
	High-rise Type I	33.05	33.53	0.48

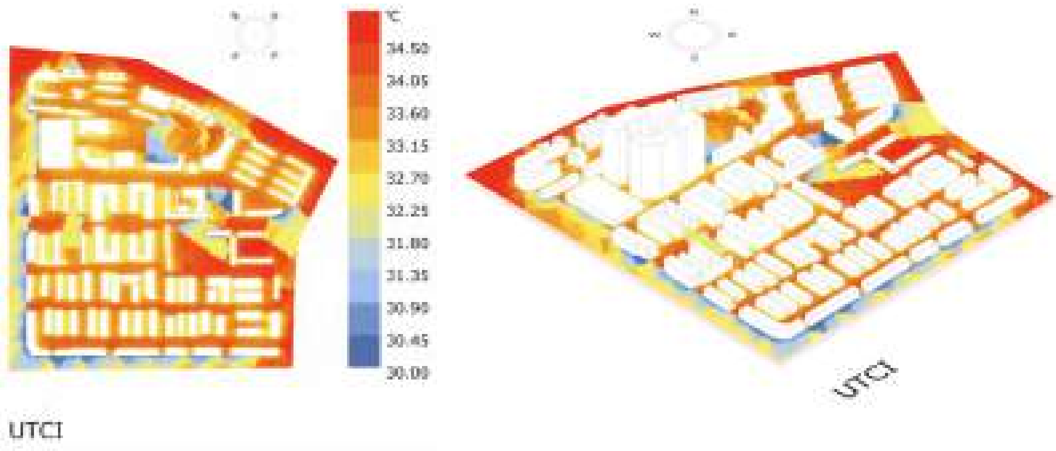

(a) Floor Plan (b) Axonometric View

Fig. 16. Simulation of outdoor thermal comfort (UTCI) on a typical summer day in Xin'an community. Note: UTCI range of 26–32 °C: moderate heat stress; UTCI range of 32–38 °C: strong thermal stress.

correlation with UTCI values ($R^2 = 0.499$), while other row-style variants received density increases of 5% to leverage beneficial shading effects. Floor area ratio adjustments increased development intensity by 0.5 for all configurations except multi-story variants, reflecting the consistent negative correlations observed between FAR and thermal comfort. Building orientation ranges were refined based on regression findings, with multi-story and high-rise Type I configurations limited to −30° to 50° ranges to optimize thermal performance.

Cluster-style layouts received comprehensive morphological enhancements reflecting their high parameter sensitivity. Building widths were increased by 5 m across all configurations to exploit the strong negative correlations with UTCI values (R^2 ranging 0.354–0.414 in high-rise configurations). Minimum floor counts were elevated by 2, 4, and 7 floors for multi-story, high-rise Type II, and high-rise Type I variants respectively, capitalizing on the consistent negative correlations between building height and thermal discomfort.

Courtyard-style developments underwent the most extensive modifications due to their complex parameter interdependence. The unified height control system was replaced with gene pool-controlled random height variations to better accommodate the varying height-width ratio sensitivities across different orientations. Building depths were increased for high-rise variants and localized open space strategies were incorporated to address the thermal accumulation issues characteristic of enclosed layouts.

4.6.2. Optimization performance results

We take the cluster-style neighborhood as an example. It is found that the cluster-style configurations achieved consistent UTCI improvements of approximately 0.45 °C through strategic implementation of the “high-density, low-coverage” principle identified in the regression analysis as indicated in Table. The combination of increased building density, enhanced floor counts, and optimized building dimensions created beneficial microclimatic conditions that substantially reduced ambient thermal stress. The superior performance of cluster-style optimization validates the counterintuitive finding that strategic densification can yield environmental benefits in point-building arrangements, which is shown in Table 8. The optimization performance results for row-style and courtyard-style configurations can be found in Appendix 1 A and 1B.

5. Discussions

5.1. Design strategy implications

The comprehensive analysis of morphological parameters and thermal comfort relationships reveals distinct design optimization strategies tailored to specific layout typologies and building height classifications. These findings provide evidence-based guidance for climate-responsive residential neighborhood planning in hot-humid environments, moving beyond conventional empirical approaches toward quantitative performance-driven design methodologies.

Row-style residential neighborhoods demonstrate layout-specific optimization requirements that vary significantly with building height. Multi-story row-style developments exhibit remarkable resilience to morphological parameter variations, with minimal correlations observed across most design variables, which suggests that building height critically modulates parameter sensitivity, with low-rise configurations maintaining thermal stability through enhanced natural ventilation and reduced thermal mass effects. However, high-rise row-style developments require careful parameter management, particularly building density control in Type II configurations where positive correlations ($R^2 = 0.499$) indicate potential thermal comfort degradation with increased density, consistent with Perini and Magliocco (Perini and Magliocco, 2014) who identified building density as a critical factor affecting outdoor thermal environments in high-density residential areas.

Cluster-style configurations present the most parameter-sensitive layout typology, offering significant optimization potential through strategic morphological adjustments. The consistent negative correlations between building density and UTCI values across all building heights (R^2 ranging 0.398–0.560) indicate that controlled density increases can enhance thermal comfort through beneficial shading effects without compromising natural ventilation. This counterintuitive finding challenges conventional low-density planning assumptions and aligns with Liu et al. (2014) who demonstrated that strategic building arrangements could improve thermal comfort through optimized shading and ventilation patterns (Liu et al., 2014). The “high-density, low-coverage” principle identified in this research provides clues regarding building layout optimization for ventilation efficiency. Courtyard-style developments require comprehensive parameter coordination due to strong interdependencies between morphological variables and thermal performance. The pronounced height-width ratio effects ($R^2 = 0.302$–0.526) demonstrate the critical importance of building proportions in courtyard configurations, supporting traditional courtyard design principles documented in vernacular architecture studies. The optimization strategy should prioritize height-width ratio increases (target range 1.5–2.5) combined with strategic building floor count adjustments, highlighting the importance of climate-specific optimization approaches.

The Bao'an case study demonstrates practical applicability of these strategies, achieving UTCI reductions of 0.2–0.6 °C across different configurations while maintaining regulatory compliance. From the perspective of global climate change, every 0.5 °C of global temperature rise will cause clearly discernible increases in the frequency and severity of heat extremes, heavy rainfall events and regional droughts (Seneviratne et al., 2021). Another existing research has also shown the city-wide installation of green roofs for buildings can lead to a UTCI reduction of 0.5 °C on average (Jiang et al., 2025). Therefore, the 0.6 °C improvement achieved by optimal configurations represents a perceptible enhancement in thermal comfort that is equivalent to city-wide use of green roof, potentially

Table 8
Comparison of Cluster-style residential neighborhood models.

	Thermal comfort optimal model	Worst thermal comfort model
Cluster-style multi-story	 Mean UTCI = 31.66	 Mean UTCI = 32.19
Sunlight Exposure Floor Plan	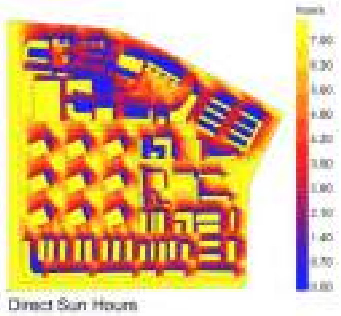	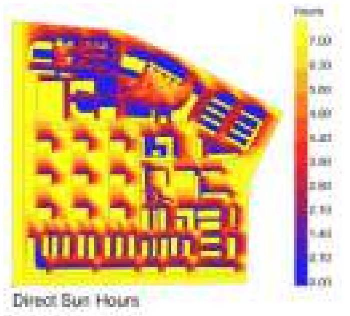
Cluster-style high-rise Type II	 Mean UTCI = 32.24	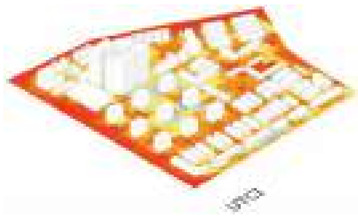 Mean UTCI = 32.70
Sunlight Exposure Floor Plan	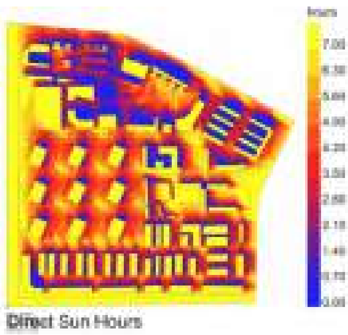	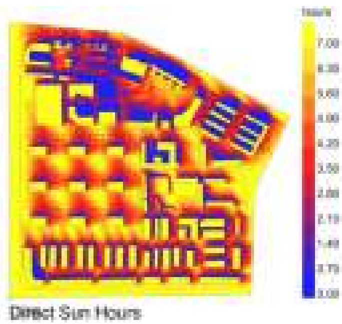
Cluster-style high-rise Type I	 Mean UTCI = 32.60	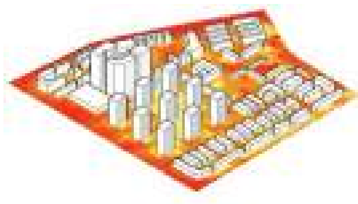 Mean UTCI = 32.98

(*continued on next page*)

Table 8 (*continued*)

	Thermal comfort optimal model	Worst thermal comfort model
Sunlight Exposure Floor Plan	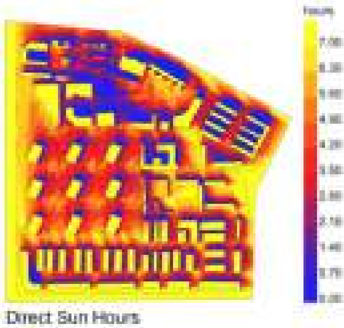	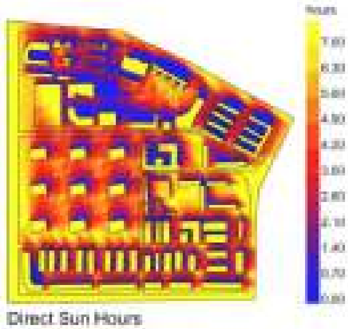

increasing the proportion of thermally comfortable occupants during peak summer conditions. This improvement is particularly significant given that optimized UTCI values of 31.66–33.05 °C fall within the moderate to strong heat stress category, where marginal temperature reductions can substantially influence outdoor activity duration and public space utilization. It is also shown from the case study that integration with existing planning frameworks requires careful consideration of regulatory constraints and implementation feasibility. The findings support density bonus mechanisms for developments demonstrating superior thermal comfort performance, particularly in cluster-style configurations where increased density correlates with environmental benefits. This approach aligns with current trends toward performance-based planning codes that prioritize environmental outcomes over prescriptive standards.

5.2. Methodological contributions and advances

The integrated parametric optimization framework developed in this research addresses fundamental limitations in conventional urban design methodologies identified by previous studies. While traditional approaches typically rely on post-design simulation for performance verification, this framework embeds environmental performance optimization directly into the design generation process, fundamentally transforming decision-making from reactive to predictive in an inverse design workflow (Chen et al., 2017).

The multi-objective optimization approach successfully reconciles competing design objectives that conventional methods struggle to balance simultaneously. The genetic algorithm implementation demonstrates consistent convergence across all nine experimental configurations, achieving thermal comfort improvements of 0.2–0.6 °C while maintaining or enhancing daylighting performance. This quantitative design optimization performance further complete recent inverse design study which reported single-objective optimization studies by Sun et al. (2023) (Sun et al., 2023) with building code compliance, demonstrating the advantages of integrated multi-constraint approach and the trade-off nature of neighborhood design optimization. The automated compliance checking system eliminates approximately 60–70% of non-conforming configurations before performance simulation, reducing computational overhead while ensuring regulatory adherence. This efficiency enables larger-scale optimization investigations within practical time constraints. Moreover, the regression analysis framework provides quantitative parameter-performance relationships that advance beyond qualitative design guidelines prevalent in existing literature. The systematic quantification of morphological impacts shown in Table 6 offers more precise design guidance than empirical recommendations in previous studies, enabling evidence-based parameter selection rather than intuitive design decisions.

The research findings both confirm and challenge established knowledge in outdoor thermal comfort optimization. The identification of building density's layout-dependent effects contradicts simplified density-thermal comfort relationships assumed in some planning guidelines. The cluster-style density benefits identified in this study provide support for theoretical framework regarding building arrangement optimization for ventilation efficiency. The quantified relationships between morphological parameters and thermal performance offer more precise design guidance than qualitative recommendations in existing literature. While previous studies typically provide directional guidance (increase/decrease specific parameters), this research establishes quantitative thresholds and correlation strengths that enable more accurate design decisions. The regression coefficients reported in Table 6 represent advances beyond descriptive analyses common in existing thermal comfort optimization literature. The integration of multiple layout typologies within a unified optimization framework addresses fragmentation issues in existing research. Previous studies typically focus on single building configurations or simplified geometric arrangements, limiting applicability to diverse urban contexts. The comprehensive analysis of row-style, cluster-style, and courtyard-style layouts provides broader design guidance than configuration-specific studies prevalent in current literature.

5.3. Limitations and future research directions

Despite significant methodological advances, several limitations constrain the current research scope and suggest priorities for future investigation. The geographic specificity of findings, while providing detailed insights for Shenzhen's hot-humid climate context, raises questions regarding transferability to other climatic regions. The morphological-thermal relationships quantified in this study reflect the particular characteristics of hot-humid subtropical climates, where ventilation enhancement and solar shading represent primary comfort improvement strategies. In contrast, cold climate regions may prioritize solar access maximization and wind protection, potentially inverting optimal parameter relationships identified herein. Similarly, hot-arid climates present distinct challenges where evaporative cooling potential and diurnal temperature variations necessitate different morphological optimization approaches. Future research should systematically investigate how the parametric relationships established in this study translate across diverse Köppen-Geiger climate classifications, developing climate-specific adjustment factors or separate optimization frameworks that account for regional variations in comfort priorities and environmental constraints. Such comparative studies would enable the development of generalized design guidelines applicable to global urban development contexts while preserving the quantitative rigor demonstrated in this research.

The environmental simulation approach adopted in this research, while computationally efficient for optimization applications, necessarily abstracts complex urban microclimate interactions. The steady-state CFD simulations may not capture temporal dynamics of urban heat island development or seasonal climatic shifts that significantly influence thermal comfort patterns. Future research should incorporate dynamic simulation approaches that better represent temporal environmental variations and their implications for year-round thermal comfort optimization. Moreover, the focus of this study on thermal comfort and daylighting objectives potentially excludes other important environmental performance criteria that influence urban sustainability. Air quality considerations, energy consumption patterns, and biodiversity support represent additional optimization dimensions that may conflict with thermal comfort priorities. Future research should develop multi-criteria optimization frameworks that simultaneously address broader sustainability objectives.

Technological advancement opportunities exist in machine learning integration to accelerate optimization processes and enable real-time design feedback. However, the current methodology relies on advanced computational tools including Rhino-Grasshopper parametric modeling, OpenFOAM CFD simulation, and genetic algorithm optimization, which require substantial technical expertise and computational resources that may limit accessibility for practicing urban planners and architects without specialized training. This technical barrier potentially constrains widespread adoption of performance-driven design approaches in routine planning practice. To address this limitation, future work should focus on developing simplified workflows and practical design guidelines that distill the quantitative findings into accessible decision-support tools. Such efforts could include lookup tables relating key morphological parameters to expected thermal comfort outcomes, rule-based design checklists derived from optimization results, or web-based simplified calculators that provide approximate performance predictions without requiring full simulation capabilities. Additionally, the development of pre-trained surrogate models using machine learning techniques could enable rapid performance estimation suitable for early-stage design exploration by non-specialists, democratizing access to evidence-based thermal comfort optimization while maintaining reasonable prediction accuracy.

The social and behavioral dimensions of thermal comfort represent underexplored territories, as cultural variations in thermal comfort expectations and outdoor activity patterns may modify optimal design solutions. Future research should expand geographical scope to include diverse climatic zones, enabling development of climate-specific optimization guidelines. In addition, future research should incorporate human-centered design methodologies that account for occupant behavior variations and cultural preferences, while developing economic assessment frameworks that quantify optimization value propositions for different stakeholder groups.

6. Conclusions

This research developed a comprehensive parametric optimization framework for residential neighborhood morphology to enhance outdoor thermal comfort in hot-humid climates, using Shenzhen as a representative case study. The methodology successfully integrated empirical data collection, parametric modeling, environmental simulation, and multi-objective optimization to generate evidence-based design strategies for climate-responsive urban planning. Key findings of this research include:

- Systematic regression analysis revealed layout-dependent parameter sensitivities, with cluster-style configurations demonstrating the strongest correlations ($R^2 = 0.398–0.625$) between design variables and thermal comfort, while row-style multi-story developments showed remarkable parameter resilience.
- Row-style layouts achieved optimal performance through density control and orientation optimization; cluster-style configurations benefited from strategic densification following the "high-density, low-coverage" principle; courtyard-style developments required coordinated height-width ratio adjustments and selective open space integration.
- Multi-objective optimization generated measurable thermal comfort enhancements of 0.2–0.6 °C UTCI reduction across all configurations while maintaining winter solstice daylighting compliance. During typical summer week conditions, optimal configurations achieved mean UTCI values of 31.66–33.05 °C compared to 32.19–33.53 °C for worst-case scenarios across various layout-building height combinations.
- The case study confirmed practical applicability, demonstrating successful integration of optimization findings with regulatory constraints and achieving predicted performance improvements in real-world urban renewal contexts.

This research provides urban planners and architects with quantitative tools for creating climate-adaptive residential environments. The parametric framework enables performance-driven design decisions that move beyond conventional empirical approaches, while the layout-specific design strategies offer implementable guidelines for hot-humid climate regions. The methodology's integration with building codes and planning regulations supports adoption in professional practice, contributing to sustainable urban development and improved outdoor thermal comfort in high-density cities.

CRediT authorship contribution statement

Pengyuan Shen: Writing – review & editing, Writing – original draft, Project administration, Methodology, Formal analysis, Conceptualization, Resources. **Xiaoni Gao:** Writing – original draft, Visualization, Software, Methodology, Investigation. **Yuting Liu:** Writing – original draft, Validation, Software, Methodology, Investigation. **Yi Zhang:** Writing – review & editing, Supervision, Methodology, Data curation. **Xing Zheng:** Writing – review & editing, Validation, Supervision, Project administration, Resources.

Declaration of competing interest

None.

Acknowledgement

This research is supported by Shenzhen Fundamental Research Program No. JCYJ20250604180231041.

Appendix A. Optimization results for row-style neighborhood in the case study

The systematic application of parameter adjustments yielded measurable thermal comfort improvements across all layout configurations. Row-style arrangements demonstrated UTCI reductions ranging from 0.2 to 0.6 °C, with the most substantial improvements occurring in high-rise Type I configurations where initial thermal stress levels were highest, as indicated in Table A1. The optimization process successfully maintained winter solstice daylighting compliance while achieving these thermal improvements, demonstrating effective multi-objective balance.

Table A1
Comparison of row-style residential neighborhood models.

	Thermal comfort optimal model	Worst thermal comfort model
Row-style multi-story		
	Mean UTCI = 31.84	Mean UTCI = 32.42
Sunlight Exposure Floor Plan	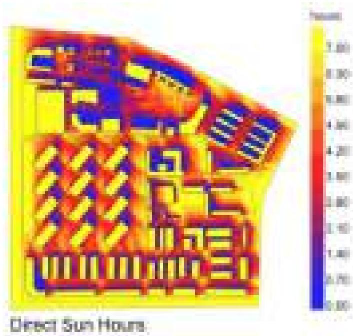	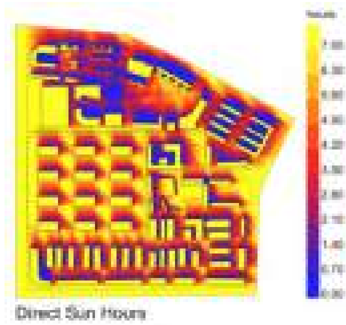

(continued on next page)

Table A1 (*continued*)

	Thermal comfort optimal model	Worst thermal comfort model
Row-style high-rise Type II	 Mean UTCI = 32.34	 Mean UTCI = 32.85
Sunlight Exposure Floor Plan	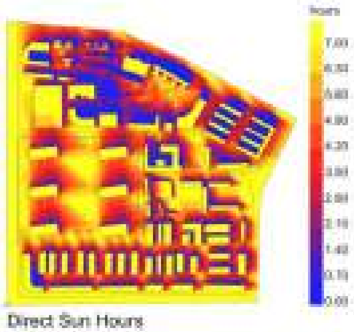	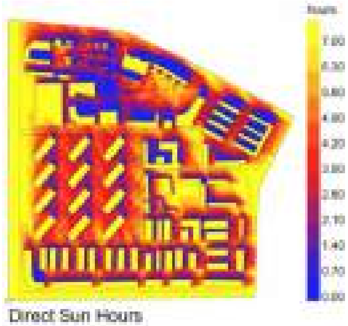
Row-style high-rise Type I	 Mean UTCI = 32.90	 Mean UTCI = 33.25
Sunlight Exposure Floor Plan	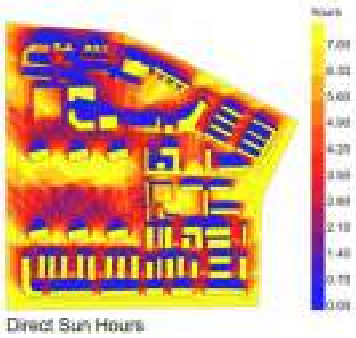	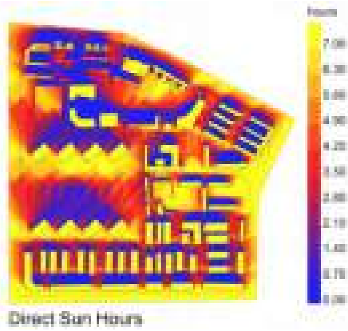

Appendix B. Optimization Results for Courtyard-style Neighborhood in The Case Study

Courtyard-style layouts realized UTCI improvements of approximately 0.4 °C through the implementation of dispersed arrangement strategies and selective open space integration, which is shown in Table A2. The transition from unified to varied building heights enabled better adaptation to local microclimatic conditions while maintaining the beneficial aspects of courtyard enclosure. The incorporation of strategic gaps in building perimeters improved natural ventilation without compromising the privacy and community benefits of courtyard arrangements.

Table A2
Comparison of courtyard-style residential neighborhood models.

	Thermal comfort optimal model	Worst thermal comfort model
Courtyard-style multi-story	 Mean UTCI = 32.35	 Mean UTCI = 32.60
Sunlight Exposure Floor Plan	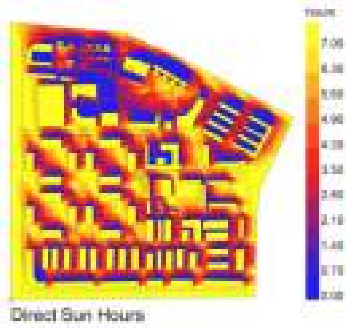	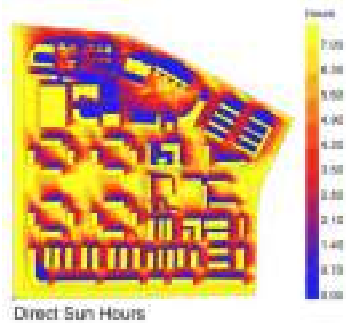
Courtyard-style high-rise Type II	 Mean UTCI = 32.62	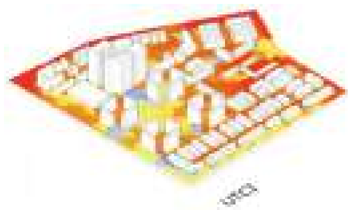 Mean UTCI = 32.90
Sunlight Exposure Floor Plan	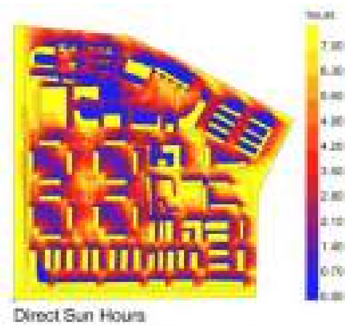	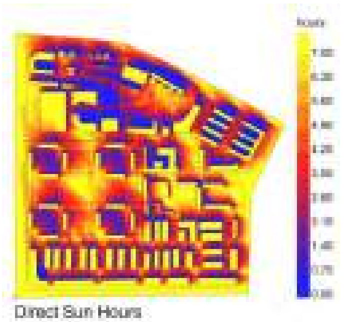
Courtyard-style high-rise Type I		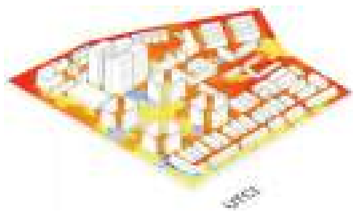

(*continued on next page*)

Table A2 (*continued*)

	Thermal comfort optimal model	Worst thermal comfort model
Sunlight Exposure Floor Plan	Mean UTCI = 33.05 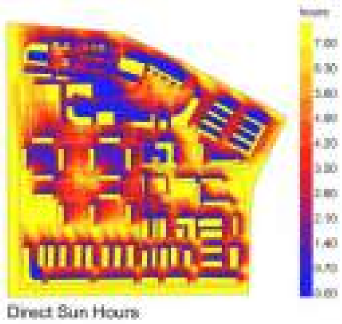 	Mean UTCI = 33.53 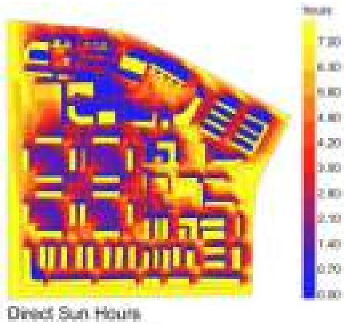

Data availability

Data will be made available on request.

References

Ahn, J., Kim, J., Kang, J., 2025. Development of an artificial intelligence model for CFD data augmentation and improvement of thermal environment in urban areas using nature-based solutions. Urban For. Urban Green. 104, 128629. https://doi.org/10.1016/j.ufug.2024.128629.

Akpan, A.N., 2023. The Effect of Commercial Building Orientations on Indoor Climate in Tropical Environments: A New Insight on Thermal Comfort Studies. Curr. Landsc. Ecol. Rep. 8, 49–61. https://doi.org/10.1007/s40823-023-00085-y.

Alharthi, M.A., Lenzholzer, S., Cortesão, J., 2025. Climate responsive design in urban open spaces in hot arid climates: a systematic literature review. Discov. Cities 2, 38. https://doi.org/10.1007/s44327-025-00069-z.

Alinasab, N., Mohammadzadeh, N., Karimi, A., Mohammadzadeh, R., Gál, T., 2025. A measurement-based framework integrating machine learning and morphological dynamics for outdoor thermal regulation. Int. J. Biometeorol. 69, 1645–1662. https://doi.org/10.1007/s00484-025-02921-8.

Ali-Toudert, F., Mayer, H., 2006. Numerical study on the effects of aspect ratio and orientation of an urban street canyon on outdoor thermal comfort in hot and dry climate. Build. Environ. 41, 94–108.

Asadi, E., da Silva, M.G., Antunes, C.H., Dias, L., Glicksman, L., 2014. Multi-objective optimization for building retrofit: A model using genetic algorithm and artificial neural network and an application. Energ. Buildings 81, 444–456. https://doi.org/10.1016/j.enbuild.2014.06.009.

Błażejczyk, K., Jendritzky, G., Bröde, P., Fiala, D., Havenith, G., Epstein, Y., Psikuta, A., Kampmann, B., 2013. An introduction to the universal thermal climate index (UTCI). Geogr. Pol. 86, 5–10.

Blocken, B., 2015. Computational Fluid Dynamics for urban physics: Importance, scales, possibilities, limitations and ten tips and tricks towards accurate and reliable simulations, Fifty Year Anniv. Build. Environ. 91, 219–245. https://doi.org/10.1016/j.buildenv.2015.02.015.

Bre, F., Gimenez, J.M., 2022. A cloud-based platform to predict wind pressure coefficients on buildings. Build. Simul. 15, 1507–1525. https://doi.org/10.1007/s12273-021-0881-9.

Broadbent, A.M., Coutts, A.M., Tapper, N.J., Demuzere, M., Beringer, J., 2018. The microscale cooling effects of water sensitive urban design and irrigation in a suburban environment. Theor. Appl. Climatol. 134, 1–23. https://doi.org/10.1007/s00704-017-2241-3.

Bröde, P., Fiala, D., Błażejczyk, K., Holmér, I., Jendritzky, G., Kampmann, B., Tinz, B., Havenith, G., 2012. Deriving the operational procedure for the Universal Thermal Climate Index (UTCI). Int. J. Biometeorol. 56, 481–494. https://doi.org/10.1007/s00484-011-0454-1.

Caldas, L.G., Norford, L.K., 2002. A design optimization tool based on a genetic algorithm. ACADIA 99 (11), 173–184. https://doi.org/10.1016/S0926-5805(00)00096-0.

Çalışkan, O., 2017. Parametric Design in Urbanism: A Critical Reflection. Plan. Pract. Res. 32, 417–443. https://doi.org/10.1080/02697459.2017.1378862.

Carlucci, S., Cattarin, G., Causone, F., Pagliano, L., 2015. Multi-objective optimization of a nearly zero-energy building based on thermal and visual discomfort minimization using a non-dominated sorting genetic algorithm (NSGA-II). Energ. Buildings 104, 378–394. https://doi.org/10.1016/j.enbuild.2015.06.064.

Chen, L., Ng, E., 2012. Outdoor thermal comfort and outdoor activities: A review of research in the past decade. Cities 29, 118–125. https://doi.org/10.1016/j.cities.2011.08.006.

Chen, Q., Zhai, Z., You, X., Zhang, T., 2017. Inverse design methods for the built environment. Routledge.

Cui, X., Li, Y., Shen, P., 2025. Beyond CFD: explainable machine learning for efficient assessment of urban morphology impacts on pedestrian level wind and thermal environment. J. Build. Perform. Simul. 2025 (05/25), 1–16. https://doi.org/10.1080/19401493.2025.2508500.

Cui, Y., Zhou, X., He, H., Fan, C., Ye, L., 2026. Assessing the coupled exposure risks of heatwaves and particulate matter: Based on the empirical analysis of 347 cities in China. J. Clean. Prod. 541, 147575. https://doi.org/10.1016/j.jclepro.2026.147575.

Davidson, S., 2013. Grasshopper-algorithmic modeling for Rhino. Lynnw. U. S.

Davtalab, J., Deyhimi, S.P., Dessi, V., Hafezi, M.R., Adib, M., 2020. The impact of green space structure on physiological equivalent temperature index in open space. Urban Clim. 31, 100574. https://doi.org/10.1016/j.uclim.2019.100574.

de Dear, R.J., Brager, G.S., 2002. Thermal comfort in naturally ventilated buildings: revisions to ASHRAE Standard 55. Spec. Issue Therm. Comf. Stand. 34, 549–561. https://doi.org/10.1016/S0378-7788(02)00005-1.

Deng, Y., Gan, D., Tang, N., Cai, Z., Li, X., Chen, S., Li, X., 2022. Research on Outdoor Thermal Comfort and Activities in Residential Areas in Subtropical China. Atmosphere 13. https://doi.org/10.3390/atmos13091357.

Dimoudi, A., Nikolopoulou, M., 2003. Vegetation in the urban environment: microclimatic analysis and benefits. Spec. Issue Urban Res. 35, 69–76. https://doi.org/10.1016/S0378-7788(02)00081-6.

Dogan, T., Kastner, P., 2021. Streamlined CFD simulation framework to generate wind-pressure coefficients on building facades for airflow network simulations. Build. Simul. 14, 1189–1200. https://doi.org/10.1007/s12273-020-0727-x.

Du, T., Turrin, M., Jansen, S., van den Dobbelsteen, A., Fang, J., 2020. Gaps and requirements for automatic generation of space layouts with optimised energy performance. Autom. Constr. 116, 103132. https://doi.org/10.1016/j.autcon.2020.103132.

Evins, R., 2013. A review of computational optimisation methods applied to sustainable building design. Renew. Sust. Energ. Rev. 22, 230–245. https://doi.org/10.1016/j.rser.2013.02.004.
Feng, K., Lu, W., Wang, Y., 2019. Assessing environmental performance in early building design stage: An integrated parametric design and machine learning method. Sustain. Cities Soc. 50, 101596. https://doi.org/10.1016/j.scs.2019.101596.
Fiala, D., Havenith, G., Bröde, P., Kampmann, B., Jendritzky, G., 2012. UTCI-Fiala multi-node model of human heat transfer and temperature regulation. Int. J. Biometeorol. 56, 429–441. https://doi.org/10.1007/s00484-011-0424-7.
Giannakopoulos, C., Bindi, M., Moriondo, M., Lesager, P., Tin, T., 2005. Climate change impacts in the Mediterranean resulting from a 2 C global temperature rise. Rep. WWF 3–5.
Givoni, B., 1998. Climate considerations in building and urban design. John Wiley & Sons.
Heydari, A., Davtalab, J., 2020. A Study of the Impact of Kharkhona on Wind Speed in the Vernacular Housing of Sistan Region. Geogr. Territ. Spat. Arrange. 10, 49–64, 10.22111/gaij.2020.5451.
Hoppe, P.R., 1999. The physiological equivalent temperature - A universal index for the biometeorological assessment of the thermal environment. Int. J. Biometeorol. 43, 71–75.
Ji, Y., Song, J., Shen, P., 2022. A review of studies and modelling of solar radiation on human thermal comfort in outdoor environment. Build. Environ. 214, 108891. https://doi.org/10.1016/j.buildenv.2022.108891.
Jiang, T., Krayenhoff, E.S., Martilli, A., Nazarian, N., Stone, B., Voogt, J.A., 2025. Prioritizing urban heat adaptation infrastructure based on multiple outcomes: Comfort, health, and energy. Proc. Natl. Acad. Sci. 122, e2411144122. https://doi.org/10.1073/pnas.2411144122.
Kamal, A., Abidi, S.M.H., Mahfouz, A., Kadam, S., Rahman, A., Hassan, I.G., Wang, L.L., 2021. Impact of urban morphology on urban microclimate and building energy loads. Energ. Buildings 253, 111499. https://doi.org/10.1016/j.enbuild.2021.111499.
Kedissa, C., Outtas, S., Belarbi, R., 2016. The impact of height/width ratio on the microclimate and thermal comfort levels of urban courtyards. Int. J. Sustain. Build. Technol. Urban Dev. 7, 174–183. https://doi.org/10.1080/2093761X.2017.1302830.
Khan, H., 2024. Microclimatic architectural design by interfacing grasshoppers and Dynamo with Rhino and Revit. Meas. Sens. 33, 101143. https://doi.org/10.1016/j.measen.2024.101143.
Kiani, H., Davtalab, J., Adib, M., Heidari, A., 2025. The Effect of Fountains and Vegetation on Temperature, Humidity and Thermal Comfort in Open Spaces with a Focus on Persian Garden: A Case Study of Kashan City. Iran. J. Energy Amp Environ. 16, 270–278. https://doi.org/10.5829/ijee.2025.16.02.09.
Ku, K.L., Liaw, J.S., Tsai, M.Y., Liu, T.S., 2015. Automatic Control System for Thermal Comfort Based on Predicted Mean Vote and Energy Saving. IEEE Trans. Autom. Sci. Eng. 12, 378–383. https://doi.org/10.1109/TASE.2014.2366206.
Lai, D., Zhou, C., Huang, J., Jiang, Y., Long, Z., Chen, Q., 2014. Outdoor space quality: A field study in an urban residential community in central China. In: 2nd Int. Conf. Build. Energy Environ. COBEE 2012 Univ. Colo. Boulder USA, 68, pp. 713–720, 10.1016/j.enbuild.2013.02.051.
Li, P., Xu, T., Wei, S., Wang, Z.-H., 2022a. Multi-objective optimization of urban environmental system design using machine learning. Comput. Environ. Urban. Syst. 94, 101796. https://doi.org/10.1016/j.compenvurbsys.2022.101796.
Li, S., Wang, M., Shen, P., Cui, X., Bu, L., Wei, R., Zhang, L., Wu, C., 2022b. Energy Saving and Thermal Comfort Performance of Passive Retrofitting Measures for Traditional Rammed Earth House in Lingnan. China, Buildings 12, 1716.
Li, J., Guo, F., Chen, H., 2024. A study on urban block design strategies for improving pedestrian-level wind conditions: CFD-based optimization and generative adversarial networks. Energ. Buildings 304, 113863. https://doi.org/10.1016/j.enbuild.2023.113863.
Liu, S., Liu, J., Yang, Q., Pei, J., Lai, D., Cao, X., Chao, J., Zhou, C., 2014. Coupled simulation of natural ventilation and daylighting for a residential community design. In: 2nd Int. Conf. Build. Energy Environ. COBEE 2012 Univ. Colo. Boulder USA, 68, pp. 686–695, 10.1016/j.enbuild.2013.08.059.
Low, S.J., Raghavan, V.S.G., Gopalan, H., Wong, J.C., Yeoh, J., Ooi, C.C., 2022. FastFlow: AI for Fast Urban Wind Velocity Prediction. In: 2022 IEEE Int. Conf. Data Min. Workshop ICDMW, pp. 147–154. https://doi.org/10.1109/ICDMW58026.2022.00028.
Machairas, V., Tsangrassoulis, A., Axarli, K., 2014. Algorithms for optimization of building design: A review. Renew. Sust. Energ. Rev. 31, 101–112. https://doi.org/10.1016/j.rser.2013.11.036.
Mandić, L., Đjukić, A., Marić, J., Mitrović, B., 2024. A Systematic Review of Outdoor Thermal Comfort Studies for the Urban (Re)Design of City Squares. Sustainability 16. https://doi.org/10.3390/su16124920.
Masoomi, Z., Mesgari, M.S., Hamrah, M., 2013. Allocation of urban land uses by Multi-Objective Particle Swarm Optimization algorithm. Int. J. Geogr. Inf. Sci. 27, 542–566. https://doi.org/10.1080/13658816.2012.698016.
Moazami, A., Carlucci, S., Nik, V.M., Geving, S., 2019. Towards climate robust buildings: An innovative method for designing buildings with robust energy performance under climate change. Energ. Buildings 202, 109378. https://doi.org/10.1016/j.enbuild.2019.109378.
Morris, K.I., Chan, A., Morris, K.J.K., Ooi, M.C.G., Oozeer, M.Y., Abakr, Y.A., Nadzir, M.S.M., Mohammed, I.Y., Al-Qrimli, H.F., 2017. Impact of urbanization level on the interactions of urban area, the urban climate, and human thermal comfort. Appl. Geogr. 79, 50–72. https://doi.org/10.1016/j.apgeog.2016.12.007.
Ng, E., Yuan, C., Chen, L., Ren, C., Fung, J.C.H., 2011. Improving the wind environment in high-density cities by understanding urban morphology and surface roughness: A study in Hong Kong. Landsc. Urban Plan. 101, 59–74. https://doi.org/10.1016/j.landurbplan.2011.01.004.
Nguyen, A.-T., Reiter, S., Rigo, P., 2014. A review on simulation-based optimization methods applied to building performance analysis. Appl. Energy 113, 1043–1058. https://doi.org/10.1016/j.apenergy.2013.08.061.
Oke, T.R., Mills, G., Christen, A., Voogt, J.A., 2017. Urban climates. Cambridge University Press.
Olgyay, V., 2016. Design with Climate. Princeton University Press. https://doi.org/10.1515/9781400873685.
Pan, W., Du, J., 2022. Effects of neighbourhood morphological characteristics on outdoor daylight and insights for sustainable urban design. J. Asian Archit. Build. Eng. 21, 342–367. https://doi.org/10.1080/13467581.2020.1870472.
Perez, R., Stewart, R., Seals, R., Guertin, T., 1988. The development and verification of the Perez diffuse radiation model, Sandia National Lab. In: (SNL-NM), Albuquerque, NM (United States). State Univ ….
Perini, K., Magliocco, A., 2014. Effects of vegetation, urban density, building height, and atmospheric conditions on local temperatures and thermal comfort. Urban For. Urban Green. 13, 495–506. https://doi.org/10.1016/j.ufug.2014.03.003.
Pompei, L., Nardecchia, F., Gugliermetti, L., Cinquepalmi, F., 2024. Design of three outdoor combined thermal comfort prediction models based on urban and environmental parameters. Energ. Buildings 306, 113946. https://doi.org/10.1016/j.enbuild.2024.113946.
Roudsari, M.S., Pak, M., Smith, A., 2013. Ladybug: a parametric environmental plugin for grasshopper to help designers create an environmentally-conscious design, pp. 3128–3135.
Santamouris, M., 2013. Using cool pavements as a mitigation strategy to fight urban heat island—A review of the actual developments. Renew. Sust. Energ. Rev. 26, 224–240. https://doi.org/10.1016/j.rser.2013.05.047.
Sauer, J.A., Muñoz-Esparza, D., 2020. The FastEddy® resident-GPU accelerated large-eddy simulation framework: Model formulation, dynamical-core validation and performance benchmarks. J. Adv. Model. Earth Syst. 12, e2020MS002100.
Seneviratne, S.I., Zhang, X., Adnan, M., Badi, W., Dereczynski, C., Luca, A.D., Ghosh, S., Iskandar, I., Kossin, J., Lewis, S., 2021. Weather and climate extreme events in a changing climate.
Shen, P., 2024. Building retrofit optimization considering future climate and decision-making under various mindsets. J. Build. Eng. 96, 110422. https://doi.org/10.1016/j.jobe.2024.110422.
Shen, P., Li, Y., Gao, X., Chen, S., Cui, X., Zhang, Y., Zheng, X., Tang, H., Wang, M., 2025a. Climate Adaptability of Building Passive Strategies to Changing Future Urban Climate: A Review. Nexus 2, 1–13. https://doi.org/10.1016/j.ynexs.2025.100061.
Shen, P., Ji, Y., Li, Y., Wang, M., Cui, X., Tong, H., 2025b. Combined impact of climate change and heat island on building energy use in three megacities in China. Energ. Buildings, 115386. https://doi.org/10.1016/j.enbuild.2025.115386.
Shi, Y., Zhang, Y., 2022. Urban morphological indicators of urban heat and moisture islands under various sky conditions in a humid subtropical region. Build. Environ. 214, 108906. https://doi.org/10.1016/j.buildenv.2022.108906.

Soflaei, F., Shokouhian, M., Abraveshdar, H., Alipour, A., 2017. The impact of courtyard design variants on shading performance in hot- arid climates of Iran. Energ. Buildings 143, 71–83. https://doi.org/10.1016/j.enbuild.2017.03.027.

Sun, R., Liu, J., Lai, D., Liu, W., 2023. Building form and outdoor thermal comfort: Inverse design the microclimate of outdoor space for a kindergarten. Energ. Buildings 284, 112824. https://doi.org/10.1016/j.enbuild.2023.112824.

Taleb, H., Musleh, M.A., 2015. Applying urban parametric design optimisation processes to a hot climate: Case study of the UAE. Sustain. Cities Soc. 14, 236–253. https://doi.org/10.1016/j.scs.2014.09.001.

Tennekes, H., 1973. The logarithmic wind profile. J. Atmos. Sci. 30, 234–238.

Tominaga, Y., Mochida, A., Yoshie, R., Kataoka, H., Nozu, T., Yoshikawa, M., Shirasawa, T., 2008. AIJ guidelines for practical applications of CFD to pedestrian wind environment around buildings, 4th Int. Symp. Comput. Wind Eng. CWE2006 96, 1749–1761. https://doi.org/10.1016/j.jweia.2008.02.058.

Tregenza, P.R., 2004. Analysing sky luminance scans to obtain frequency distributions of CIE Standard General Skies. Light. Res. Technol. 36, 271–279.

Wai, C.Y., Tariq, M.A.U.R., Chau, H.-W., Muttil, N., Jamei, E., 2024. A Simulation-Based Study on the Impact of Parametric Design on Outdoor Thermal Comfort and Urban Overheating. Land 13. https://doi.org/10.3390/land13060829.

Wang, Y., Guo, J., Jiang, Y., Sun, C., 2024. Multi-objective optimization of buildings in urban scale for early stage planning and parametric design. Sustain. Cities Soc. 113, 105714. https://doi.org/10.1016/j.scs.2024.105714.

Wang, M., Ma, H., Zheng, X., Han, C., Shen, P., 2025. Two-way coupled numerical simulation between outdoor thermal environment and PM2.5 in urban blocks. Build. Environ. 275, 112821. https://doi.org/10.1016/j.buildenv.2025.112821.

Xu, X., Wu, Y., Wang, W., Hong, T., Xu, N., 2019. Performance-driven optimization of urban open space configuration in the cold-winter and hot-summer region of China. Build. Simul. 12, 411–424. https://doi.org/10.1007/s12273-019-0510-z.

Yang, Y., Zhou, D., Wang, Y., Meng, X., Gu, Z., Xu, D., Han, X., 2022. Planning method of centralized greening in high-rise residential blocks based on improvement of thermal comfort in summer. Sustain. Cities Soc. 80, 103802. https://doi.org/10.1016/j.scs.2022.103802.

Yi, Y.K., Malkawi, A.M., 2009. Optimizing building form for energy performance based on hierarchical geometry relation. Autom. Constr. 18, 825–833. https://doi.org/10.1016/j.autcon.2009.03.006.

Yuan, C., Ng, E., 2012. Building porosity for better urban ventilation in high-density cities – A computational parametric study. Build. Environ. 50, 176–189. https://doi.org/10.1016/j.buildenv.2011.10.023.

Yuan, C., Zhu, R., Tong, S., Mei, S., Zhu, W., 2022. Impact of anthropogenic heat from air-conditioning on air temperature of naturally ventilated apartments at high-density tropical cities. Energ. Buildings 268, 112171. https://doi.org/10.1016/j.enbuild.2022.112171.

Zaker Vafaee, N., Sandani, M., Khamene, T.A., Tagnocchetti, M., Izumi, B., Finocchiaro, L., 2022. Integrating energy in the conceptual design stage to optimize building form. In: Proc. 63rd Int. Conf. Scand. Simul. Soc. SIMS 2022 Trondheim Nor. Sept. 20-21 2022. Linköping University Electronic Press.

Zhai, Z. John, Previtali, J.M., 2010. Ancient vernacular architecture: characteristics categorization and energy performance evaluation. Energ. Buildings 42, 357–365. https://doi.org/10.1016/j.enbuild.2009.10.002.

Zhen, M., Zou, W., Zheng, R., Lu, Y., 2022. Urban outdoor thermal environment and adaptive thermal comfort during the summer. Environ. Sci. Pollut. Res. 29, 77864–77883. https://doi.org/10.1007/s11356-022-21162-5.

Zheng, X., Yang, J., 2021. CFD simulations of wind flow and pollutant dispersion in a street canyon with traffic flow: Comparison between RANS and LES. Sustain. Cities Soc. 75, 103307. https://doi.org/10.1016/j.scs.2021.103307.

Zheng, X., Yang, J., 2022. Impact of moving traffic on pollutant transport in street canyons under perpendicular winds: A CFD analysis using large-eddy simulations. Sustain. Cities Soc. 82, 103911. https://doi.org/10.1016/j.scs.2022.103911.

Zheng, H., Yuan, P.F., 2021. A generative architectural and urban design method through artificial neural networks. Build. Environ. 205, 108178. https://doi.org/10.1016/j.buildenv.2021.108178.